

Electronic Properties of Semiconductor Nanowires

L. C. Lew Yan Voon^{1,*}, Yong Zhang², B. Lassen³, M. Willatzen³, Qihua Xiong^{4,†}, and P. C. Eklund⁴

¹Department of Physics, Wright State University, 3640 Colonel Glenn Hwy, Dayton, Ohio 45435, USA

²National Renewable Energy Laboratory, Golden, Colorado 80401, USA

³Mads Clausen Institute, University of Southern Denmark, Alsion 2, Alsion, DK-6400 Sønderborg, Denmark

⁴Departments of Physics and Material Science and Engineering, Pennsylvania State University, University Park, Pennsylvania 16802, USA

This paper provides a review of the state-of-the-art electronic-structure calculations of semiconductor nanowires. Results obtained using empirical $k \cdot p$, empirical tight-binding, semi-empirical pseudopotential, and with *ab initio* methods are compared. For conciseness, we will restrict our detailed discussions to free-standing plain and modulated nanowires. Connections to relevant experimental data, particularly band gaps and polarization anisotropy, will be made since these results depend crucially on the electronic properties. For completeness, a brief review on the synthesis of nanowires is included.

Keywords: Semiconductor Nanowires, Electronic Properties, Optical Properties, Theoretical Methods.

CONTENTS

1. Introduction	1
2. Experimental Details	3
2.1. Growth and Synthesis	3
2.2. Electronic and Optical Properties	6
2.3. Other Properties	6
3. Theoretical Methods	6
3.1. $k \cdot p$ Method	6
3.2. Tight-Binding Method	8
3.3. First-Principles Methods	8
3.4. Empirical Pseudopotential Methods	10
4. Electronic Properties	10
4.1. Quantum Wires	10
4.2. Nanowires	11
4.3. Modulated Nanowires	20
4.4. Quantum Rods	20
5. Polarized Optical Properties	21
5.1. Nanowires	21
5.2. Quantum Rods	22
6. Summary	23
Acknowledgments	23
References and Notes	23

1. INTRODUCTION

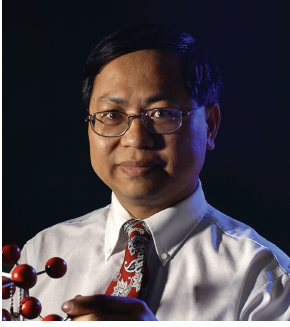
The study of inorganic semiconductor nanostructures advanced from quantum wells to (embedded) quantum wires to quantum dots roughly from the 1970s to the 1990s with the development of epitaxial growth and lithographic

methods. The increasing degree of quantum confinement had allowed to substantially alter the physical properties leading to fundamentally new physics under reasonable external conditions. Examples include the quantum Hall effect,^{1,2} ballistic conductance,³ and Coulomb blockade.^{4,5} In turn, this has generally led to improved physical properties such as higher electron mobility for nanowires,⁶ reduced nonradiative recombination,⁷ and lower lasing threshold as the degree of confinement increases,⁸ or the design of new devices such as nanowire solar cells,⁹ infrared photodetectors,¹⁰ and field-effect transistors.¹¹ More recently, however, the development of chemical synthesis and bottom-up methods has expanded the study of free-standing nanowires. The potential of these new techniques is that they involve much simpler chemical synthesis methods, are relatively inexpensive, and produce single-crystal nanowires of high quality and purity. A nanowire or quantum wire can be defined as a structure exhibiting quantum confinement effects in the plane perpendicular to the wire axis and free-electron-like behaviour along the latter. Typical geometrical dimensions are 1–100 nm linear lateral dimensions and microns in length. The starting point for interpreting optical and transport experiments on any material system is a knowledge of the electronic structure. While the formal basis for the latter is based upon the quantum-mechanical Schrödinger equation, explicit solutions is still a research area.

The goals of this article are multi-fold. One is to provide an overview of the literature—though this is becoming an increasingly difficult task. Thus, we will not attempt to

*Author to whom correspondence should be addressed.

†Present address: Harvard University, 12 Oxford Street, Cambridge, MA 02138, USA.



Lok C. Lew Yan Voon received the B.A. degree from the University of Cambridge, UK in 1987, the M.Sc. degree from the University of British Columbia, Canada in 1989, and the Ph.D. degree from Worcester Polytechnic Institute, USA in 1993, all in physics. After an Alexander von Humboldt postdoctoral fellowship at the Max Planck Institute for Solid State Physics in Stuttgart, Germany in the group of Professor Dr. Cardona, he joined the physics faculty at Worcester Polytechnic Institute. In 2004, he became professor and chair of the physics department at Wright State University in Dayton, Ohio. Dr. Lew Yan Voon received the NSF CAREER award in 2000 and has published over 75 papers to date.



Dr. Yong Zhang is a Senior Scientist at National Renewable Energy Laboratory (NREL). He received his M.S. degree in Semiconductor Physics in 1985 from Xiamen University, and Ph.D. degree in Solid State Physics in 1994 from Dartmouth College. His research areas include the electronic and optical properties of bulk semiconductors, inorganic and inorganic-organic hybrid nanostructures, doping, defects, and spontaneous ordering or composition modulation in semiconductors, propagation of electron waves or light in anisotropic crystals, using various experimental and theoretical techniques (e.g., laser spectroscopy, first-principles and empiric electronic structure calculation). He has authored or co-authored over 120 publications in these areas.

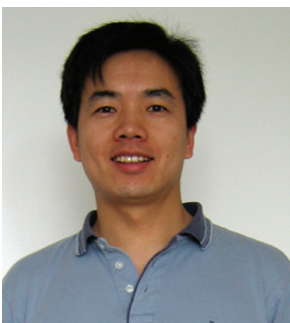
University of Southern California
IP : 128.125.153.210
Wed, 20 Feb 2008 02:52:03



Benny Lassen received both his M.Sc. degree in mathematics (2002) and his Ph.D. degree in mathematical modelling (2005) at the University of Southern Denmark. After the Ph.D. degree he worked one year at Lund University financed by a Villum Kann Rasmussen postdoctoral stipend. He is now working as an assistant professor at the University of Southern Denmark. His main area of research is nanoscale semiconductor heterostructures, specifically, electronic bandstructures, transport, strain and piezoelectric effects.



Morten Willatzen received the M.Sc. degree in theoretical physics at the University of Aarhus, Denmark (1989) and the Ph.D. degree in semiconductor physics at the Niels Bohr Institute, University of Copenhagen, Denmark (1993). He has been in postdoctoral jobs at the Max-Planck Institute, Stuttgart, Germany and TeleDanmark Research, Hørsholm, Denmark in the period 1993–1995. MW has been 8 years in industry working in telecommunications and fluid systems. Presently, he is a professor and group leader of mathematical modelling at the Mads Clausen Institute, University of Southern Denmark. MW's research interests include: solid state physics—in particular—quantum-confined structures and applications to semiconductor laser amplifiers, flow acoustics, transducer modelling, and modelling of thermo-fluid systems.



Qihua Xiong received his Ph.D. degree in materials science from The Pennsylvania State University in 2006. His Ph.D. thesis research with Professor Peter Eklund was focused on the phonon properties of semiconducting nanowires studied by Raman spectroscopy. His research work elaborated how size (diameter) and shape (cross section, aspect ratio, etc.) affect the phonon properties in nanowires, via studies of laser-induced Fano resonance, activation of surface optical phonon scattering and nano-antenna effect in nanowires. He also studied the nanomechanical properties of nanowires by nano-indentation and force-deflection spectroscopy. Dr. Xiong is currently working as a postdoctoral researcher with Professor Charles Lieber at Harvard University.



Professor P. C. Eklund received his A.B. Degree (Physics) from the University of California at Berkeley and his M.Sc. and Ph.D. degrees (Solid State Physics) from Purdue University. He was at MIT for two years of post doctoral experience. His University career began at the University of Kentucky where he was a Professor and Associate Director for at the Center for Applied Energy Research. He then moved to Penn State University in 1999 where he is a Distinguished Professor and holds a joint appointment in the departments of Physics and Materials Sci. and Eng'ng. He is a *Fellow* of the American Physical Society (1990) and was awarded the *Graffin* prize by American Carbon Society (2005). He also received the University Research Professorship award (1998) at the University of Kentucky. Professor Eklund is known for his research in nanomaterials synthesis and physical properties, particularly optical properties. He has published over 300 research papers in refereed

journals, 2 Research Monographs, over 20 Review articles and Book Chapters. He has 6 US Patents issued and 6 pending. Recently, his research has focused on hydrogen storage materials, fundamental physics of semiconducting nanowires, carbon nanotubes, graphene and sensor devices from these filaments and sheets. He is also the President of CarboLex, Inc. (founded 1997), the first company to be involved in the production and sale of carbon nanotubes.

cite the whole literature, rather a cross section of the key works. Furthermore, a number of reviews have appeared in recent years. The older literature on GaAs and InAs nanowhiskers was reviewed in an article in 1995.¹² A condensed communication on the general synthesis of compound semiconductor nanowires was reported by Duan and Lieber in 2000.¹³ The group of Peidong Yang has written a number of reviews,^{14,15} mostly about the synthesis with a brief overview of the physical properties of nanowires. An extensive review of materials, properties, and devices up to 2003 can be found in the two-volume book edited by Wang.¹⁶ In 2004, Bowler reviewed mostly the transport properties.¹⁷ The October 2006 issue of *Materials Today* is devoted to nanowires and nanotubes.¹⁸ Hence, we focus our review on one area that has not been properly reviewed—that of the calculation of electronic properties.

We also aspire to provide the experimentalists (and others) with an overview of the theoretical landscape, both in terms of models and results. For example, how do *ab initio* and empirical techniques compare in terms of the underlying physics and of accuracy? In the process, we hope to support our belief that, even though band-structure theory is old and there are many papers on bulk, quantum-well, and quantum-dot systems, the study of quantum wires or nanowires is still filled with opportunities and challenges.

We divide the current review into three parts. The first presents a brief overview of experiments on nanowires, relevant to discussing the electronic properties. The second part provides a succinct exposition of the various theoretical tools that have been employed to investigate the electronic structure of nanowires. Finally, we give a few representative results in the third part, particularly as they apply to understanding optical properties.

2. EXPERIMENTAL DETAILS

The first conceptualization of a quantum wire (QWR) is usually attributed to a 1980 paper by Sakaki.⁶ The most

direct way of studying the electronic properties is by making nanowires of different size, shape, and orientation and measuring the optical spectra.

2.1. Growth and Synthesis

In the rest of the article, the term *nanowires* (NW's) will be restricted to free-standing homogeneous wires with very large aspect ratio (typical experimental length being of the order of microns which is treated theoretically as infinite). *Quantum wires* (QWR's) will refer to the embedded structures. *Quantum rods* (QR's) or *nanorods* will refer to one-dimensional nanostructures with small aspect ratio (typically less than a few tens). The above choices of definitions are mostly of historical origin.

One-dimensional (1D) nanostructures have been grown in various shapes and geometries: embedded with square cross-section,¹⁹ T-shaped,²⁰ strain induced lateral confinement in quantum wells,²¹ V-groove shaped,²² plain free-standing,²³ nanobelts,²⁴ quantum rods,²⁵ core-shell,²⁶ axially modulated,^{27–29} and nanotubes.³⁰ The variety reflects not only the curiosity in how properties change but also the experimental constraints. For example, core-shell structures protect the inner core from surface effects inherent in a free-standing nanowire. InP-based systems are preferred over AlGaAs due to the ease of oxidation of the latter. CdS nanowires are preferred over GaAs ones for the polarized photoluminescence studies due to the higher emission efficiency of the former.

We will now summarize the growth of various types of one-dimensional nanostructures, with emphasis on nanowires.

2.1.1. Quantum Wires

In 1982, one-dimensional structures displaying quantum confinement of two dimensions were reported by Petroff et al.¹⁹ Those were GaAs quantum-well wires with submicron dimensions obtained using molecular beam epitaxy

(MBE) of GaAs and $\text{Ga}_{1-x}\text{Al}_x\text{As}$. Transmission electron microscopy (TEM) showed them to be single crystal, defect-free wires, with cross-section dimensions as small as $20 \times 20 \text{ nm}^2$.

Quantum wires can also be formed at the intersection of two quantum wells and have been named T-shaped QWR's.²⁰ The basic process has been to grow one set of quantum wells (via MBE), then cleave the sample, and finally, grow the second set of intersecting quantum wells. Such QWR's are expected to have high structural quality.

Another type of QWR that was popular for a while was of V shape. High quality V-groove quantum wires of nanometer cross section have been grown by low pressure organometallic chemical vapor deposition (MOCVD) techniques.²² This was achieved at a pressure of 20 mbar on a (001) GaAs substrate and with the latter at a temperature between 600 and 765 °C. The structural parameters and quality were initially ascertained using conventional and high resolution transmission electron microscopy (HRTEM), and by low-temperature cathodoluminescence.²² V-groove QWR's of InGaAs with {111}A InP facets and on (001) oriented InP:S substrates have also been grown by low-pressure MOCVD.³¹

2.1.2. Nanowires

Nanowires that have been grown or synthesized include AlN,^{32, 33} CdS,^{34–36} CdSe,^{34, 37–40} GaAs,^{34, 41–43} GaN,^{44–48} GaP,³⁴ Ge,²³ InN,⁴⁹ InAs,^{34, 50, 51} InP,^{34, 52–55} α -MnS,⁵⁶ Si,^{23, 57, 58} SiC,⁵⁹ ZnO,^{60–65} ZnS,^{34, 66–68} and ZnSe.^{34, 69, 70} These nanowire sizes range from a few hundred to a few nm. Apparently, the ultimately thin wire would be a linear chain of atoms. However, the thinnest known semiconductor wire is perhaps the subnano meter [0001] zigzag atomic chain of wurtzite ZnTe (with only four atoms per period).⁷¹ The ZnTe wires are coordinated or “passivated” by organic molecules pda, and form a perfect wire array or a crystal $\text{ZnTe}(\text{pda})_{0.5}$. A list of the smallest cross-section ones is given in Table I.

It is practical to distinguish between growth mechanisms and growth methods. The growth mechanism is the general phenomenon that explains how the thermodynamics and kinetics ensure that nanowires with a filament morphology and single crystallinity are obtained;¹⁵ while the growth methods refer to the experimental chemical processes that employ the appropriate environment to synthesize the nanowires with anticipated morphology and crystallinity. So it is possible to utilize different chemical processes to grow different species of nanowires using the same growth mechanism. Many NW's, e.g., a wide range of oxides, have been grown successfully without clear understanding of the growth mechanism. Nevertheless, it is still crucial to understand the underlying growth mechanism such that rationally controlled growth, in terms

Table I. Smallest nanowires reported. C = cubic, H = hexagonal, R = rocksalt.

Material	Structure	Orientation	Smallest size (nm)	Reference
Si	C	[111]	1.3	[58]
Ge	C	[111]	3	[23]
β -SiC	C	[111]	90	[59]
GaAs	C	[111]	3	[34]
GaP	C	[111]	3	[34]
InN	C	[001]	10	[49]
InP	C		3	[72]
InAs	C	[100], [110]	15	[50]
	C	[111]	3	[34]
CdS	H	[100], [002]	3	[34]
CdSe	H	[10 $\bar{1}$ 0], [0001]	70	[40]
	H	[110]	3	[34]
ZnO	H	[0001]	20	[62]
ZnS	C	[111]	4	[34]
ZnSe	C	[111]	3	[34]
	C	[112]	3	[73]
AlN	W	[0001]	10	[33]
GaN	H	[100], [001]	4	[44]
α -MnS	R		70	[56]

of size, shape and architecture of heterostructures, will be achieved. As a matter of fact, several mechanisms behind different growth methods have not been completely understood until recently. For example, the vapor-liquid-solid (VLS) mechanism⁷⁴ was first proposed to explain the growth of micrometer diameter whiskers from a liquid droplet. It was the primary mechanism cited to describe the nanowires grown when a particle was observed at one end of the nanowires. However, only recently have real-time observations of the VLS growth stages been demonstrated via *in-situ* TEM.⁷⁵ In 2004, the very idea that VLS growth automatically applies to all NW's found with a metal particle at one end has been challenged.^{76, 77} Instead, even though metal “seed” particles were involved in the growth, a vapor-solid-solid mechanism was proposed to explain some III–V compound NW's growth by chemical beam epitaxy (CBE).^{76, 77} Several growth mechanisms involving liquid phase growth environment have also been explored, e.g., Trentler et al.⁷⁸ synthesized several III–V compound (InAs, InP and GaAs) nanowires by a solution phase synthesis, i.e., the so-called solution-liquid-solid (SLS) mechanism. Depending upon the solvent, this has also been referred to as the solvothermal or hydrothermal method.⁷⁹ The other similar mechanism is called super-critical fluid-liquid-solid mechanism, in which a super-critical solution was used to dissolve source materials (precursors and other agents) for subsequent nanowire growth.^{80, 81} Among different nanowire growth mechanisms, the VLS growth mechanism is so far the most versatile and extensively used to grow a variety of semiconducting nanowires. VLS was proposed several decades ago by Wagner and Eillis⁷⁴ to explain the growth of semiconducting Si whiskers using impurity metal particles, such as Au, Ni, Cu, etc. The as-grown whiskers exhibited diameters in the range of a

few microns and were single crystalline without dislocations. Therefore, the conventional screw dislocation crystal growth mechanism cannot explain the 1D growth.⁷⁴ It was later found that Ge,⁸² InAs and GaAs¹² whiskers could also be grown via the same mechanism. In this context, whisker refers to single crystalline form filament in μm or sub- μm diameter regime. Morales and Lieber²³ demonstrated that much smaller diameter Si and Ge nanowires (3–20 nm in diameter) and several μm in length could be grown using a pulsed laser to vaporize the semiconductor and Fe needed in the growth seed. This so-called pulsed laser vaporization (PLV) method provides nanometer-sized Fe particles and Si/Ge vapor supply. It was this landmark paper that arouse worldwide research on semiconducting nanowires. Besides PLV method,^{13, 68, 83} several other methods such as chemical vapor deposition (CVD),^{84, 85} MOCVD,⁸⁶ vapor transport using solid source or molecular precursors^{87, 88} and physical evaporation^{89, 90} have been used to provide the necessary vapor source to initiate the VLS growth. In Figures 1–3, we show examples of morphology and crystallinity of nanowires grown by PLV method based on the VLS mechanism. Figure 1 is a scanning electron microscope (SEM) image of GaP nanowires dispersed on a Si substrate. Figure 2 is an HRTEM image of a Si nanowire growth along the $[111]$ direction. Figures 3(a and b) are TEM images of GaP nanowires; the growth tip was clearly identified, which is a proof of VLS growth. Figure 3(c) is a typical selective-area electron diffraction pattern indexed as a two-fold symmetry $[\bar{1}12]$ pattern. The growth orientation is $[111]$.

2.1.3. Nanobelts

Nanobelts or nanoribbons are basically nanowires with a rectangular cross section of larger aspect ratio. They were first synthesized in 2001 by the group of Wang.²⁴ So far, even the smallest diameter is typically outside the quantum-confinement regime.

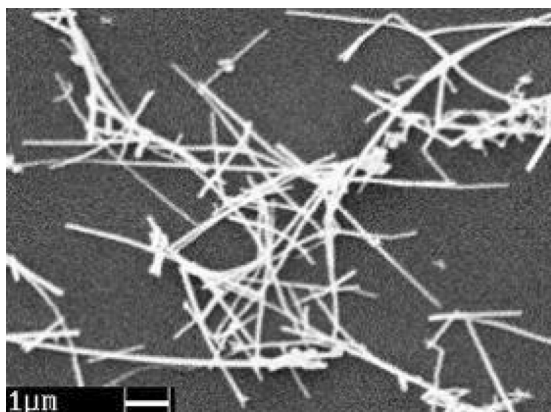


Fig. 1. SEM image of GaP nanowires dispersed on Si substrate grown by PLV method.

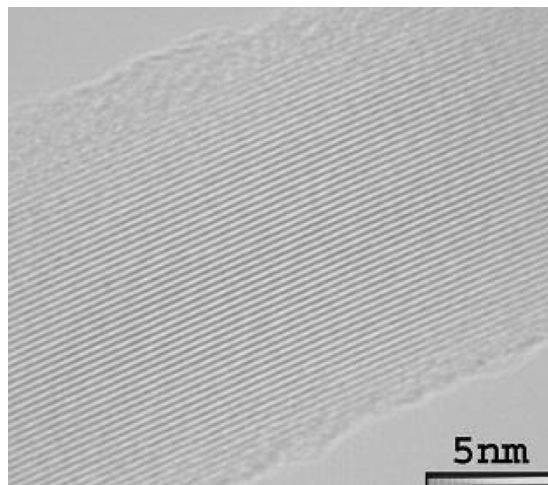


Fig. 2. HRTEM image of typical Si nanowires grown by PLV method. A thin layer of amorphous oxide was observed.

2.1.4. Nanorods

The first synthesis of nanorods with very narrow size distribution was reported by the group of Alivisatos in 2001^{37, 91} for CdSe. GaN nanorods have been identified with a $\langle 1\bar{1}00 \rangle$ axis and rectangular cross-sections of order 100–150 nm.⁹² Other nanorods made include AlN,³² InP,^{93, 94} PbSe,⁹⁵ SiCN,²⁵ and ZnO.^{63, 96, 97}

2.1.5. Modulated Nanowires

The first type made was the radial or core/shell type. For example, InAs/A-B⁹⁸ were made via high-temperature colloidal synthesis, Si/Ge,²⁶ GaN/InGaN⁹⁹ and CdS/ZnS¹⁰⁰

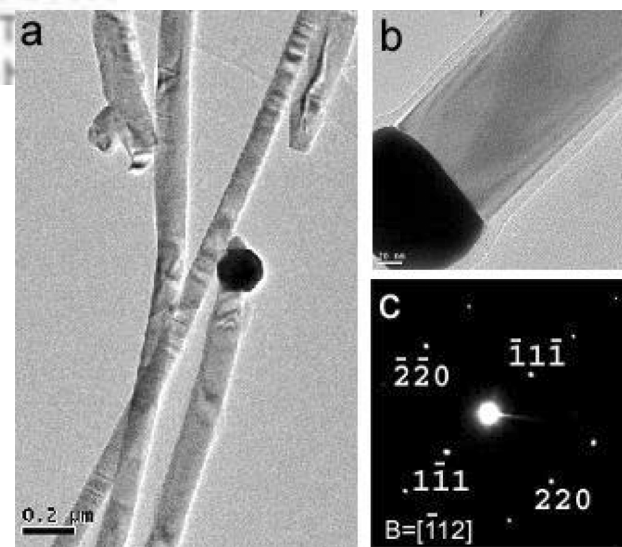


Fig. 3. (a) and (b) TEM images GaP nanowires with a $[111]$ growth direction. The growth tips are clearly identified. (c) SAED pattern from nanowire shown in (b). A two-fold symmetry pattern was observed and indexed as a $[\bar{1}12]$ zone axis pattern.

via MOCVD, and GaAs/AlGaAs via selective-area metalorganic vapor phase epitaxy¹⁰¹ and VLS.³⁶ Typical dimensions achieved were, as an example, a CdS core of 20–30 nm with a 10 nm shell.

One of the most exciting new nanostructures is the axially-modulated nanowire.^{27–29, 42, 102, 103} Various growth techniques, most of which are based upon a nano-cluster catalyst, have recently been used to form nanowires with longitudinal modulation. The material systems considered were GaAs/GaP,²⁷ Si/SiGe,²⁸ InAs/InP,²⁹ ZnSe/CdSe¹⁰² (the latter using atomic-layer deposition) and AlGaAs/GaAs.⁴² Typical dimensions have been nanowire radii of 20–40 nm and layer widths of 1.5–100 nm. It has been predicted that these structures might find applications as nano bar codes, waveguides, lasers, and LEDs. It has been speculated²⁷ that the nanowire superlattice (NWSL) is an improvement over the plain nanowire¹⁰⁴ due to the coupling of the superlattice longitudinal confinement to the nanowire radial confinement. Among the characteristic properties reported so far, we note the extremely polarized photoluminescence²⁷ of a NWSL and the nonohmic conductance of a NWSL with a single barrier layer.¹⁰⁵ Due to the large radii of the structures grown so far, there is not yet any experimental evidence of novel quantum phenomena in these structures.

2.1.6. Nanotubes

For completeness, we mention that nanotubes have now been made of, for example, ZnO,¹⁰⁶ and GaN.¹⁰⁷ The ZnO nanotubes have a hexagonal wurtzite phase with $a = 0.325$ nm and $c = 0.521$ nm. The wall thickness was as small as 4 nm and tube diameters ranged 30–100 nm. We will not consider nanotubes any further in this article.

2.2. Electronic and Optical Properties

The optical spectrum of a nanowire would not only elucidate the physics and provide a characterization of the nanowire, but is also important in designing photonic devices. It tends to be one of the cleanest characterization tools available since it relates so closely to the electronic properties and is nondestructive. Not surprisingly, numerous such studies have been conducted such as optical absorption,⁶⁸ photoluminescence (PL),⁶⁸ and Raman spectroscopy.¹⁰⁸

There have been a few measurements of the size dependence of the band gap. Various measurements (e.g., PL and scanning tunneling spectroscopy) have been reported for Si,^{57, 109} and size-dependent PL for InP^{52, 53} and CdSe³⁸ nanowires, with a blue shift measured for diameters smaller than 20 nm. Dependence of properties on nanowire morphology is less studied. Examples are for InP,¹¹⁰ ZnO¹¹¹ and CdS.¹¹² There are also few studies on the alloy dependence of the band gap.³⁹

A problem of current interest is the nature of the light polarization emitted or absorbed by quantum rods and nanowires. The earliest experimental report of linearly-polarized emission appears to be in 1989^{113, 114} from an (AlGa)As–GaAs quantum-well-wire array made by MBE. The polarization dependence of the photoluminescence excitation (PLE) data was attributed to the different properties of light holes (LH's) and heavy holes (HH's) in the quantum-confined regime.¹¹³ Additionally, similar studies have been performed on T-shaped¹¹⁵ and V-grooved¹¹⁶ QWR's.

The above problem was also studied for free-standing nanowires, first of zincblende structure, then also of wurtzite structure. Wang et al.¹⁰⁴ reported room temperature linearly-polarized emission from *single* InP nanowires of 0.91 ± 0.07 (predominantly growth-direction polarized); the nanowires had diameters in the range 10–50 nm. Similar results have now been reported for Si^{117, 118} nanowires. Wurtzite nanowires that have been investigated include CdSe,^{40, 119} GaN,¹²⁰ and ZnO.⁶⁵ Linear polarization has also been observed for AlGaAs/GaAs core-shell nanowires.^{27, 36}

A related study is of the optical polarization for quantum rods. Hu et al.³⁷ studied CdSe QR's with aspect ratios from 1 to 30 and with radii of 2–3 nm. Their polarized luminescence experiments gave a transition to z -polarized optical emission at an aspect ratio of 1.5–2. Similar polarization data were obtained for ZnO QR's.⁹⁷

2.3. Other Properties

For completeness, we briefly mention a few characterization techniques that have been used to obtain other properties of nanowires. Current–voltage plots have been used to distinguish between homogeneous InAs and InAs/InP modulated nanowires.²⁹ Longitudinal photoconductivity has been used on GaAs/AlGaAs V-groove QWR's as a method that combines absorption spectroscopy with carrier transport.¹²¹ Relaxation dynamics in CdSe quantum rods were studied using femtosecond transient absorption spectroscopy.¹²² Gate-dependent transport measurements on intrinsic (2.13×10^{-11}) and B-doped (9.54×10^{-9}) SiNW yielded mobilities of 5.9×10^{-3} cm²/(Vs) and 3.17 cm²/(Vs).⁸⁴ More recently, better than bulk mobilities [650 cm²/(Vs)] have been obtained for GaN nanowires using a similar technique by the same group.¹²³ Carrier densities were estimated from the total charge and the threshold voltage needed to deplete the NW.

3. THEORETICAL METHODS

3.1. $k \cdot p$ Method

The proper formalism is the one proposed by Burt¹²⁴ for the envelope-function approximation although $k \cdot p$ theory was in use several decades before based on more

heuristic procedures, for a detailed account refer, e.g., to Bastard.¹²⁵ The usual starting point in the derivation of $k \cdot p$ multiband Hamiltonian equations is the one-particle Schrödinger equation:

$$\left\{ -\frac{\hbar^2}{2m_0} \nabla^2 + V(\vec{r}) \right\} \psi = E\psi \quad (1)$$

where m_0 is the free-electron mass, ∇^2 is the Laplacian and $V(\vec{r})$ is the potential of all other charged particles (atoms and other electrons) in the system (in a mean-field approximation). The central idea in $k \cdot p$ theory is to make an envelope-function expansion of the wave function and then derive a set of coupled equations for the envelope functions. The envelope function expansion is given by:

$$\psi(\vec{r}) = \sum_n F_n(\vec{r}) u_n(\vec{r}) \quad (2)$$

where the set u_n is a complete set of periodic functions with a given periodicity (usually the zone-center solutions of a bulk material). Disregarding non-local effects^{124, 126} the set of coupled equations for the envelope functions is found to be:

$$-\frac{\hbar^2}{2m} \nabla^2 F_n(\vec{r}) - \frac{i\hbar}{m} \sum_l \vec{p}_{nl} \cdot \vec{\nabla} F_l(\vec{r}) + \sum_l H_{nl}(\vec{r}) F_l(\vec{r}) = E F_n \quad (3)$$

where

$$\vec{p}_{nl} = -i\hbar \int u_n^* \vec{\nabla} u_l d^3r, H_{nl}(\vec{r}) = \frac{1}{V_c} \int u_n^* \left\{ -\frac{\hbar^2}{2m_0} \nabla^2 + V(\vec{r}) \right\} u_l d^3r$$

and V_c is the volume of the periodic cell.¹²⁷ Löwdin perturbation theory¹²⁸ can be used to reduce the above infinite set of equations to a finite set, e.g., one-band (effective-mass equation, conduction band), four-band (heavy- and light-holes), six-band (heavy-, light-, and split-off-holes), etc. As an example, the one-band conduction equation (S states) for a heterostructure reads:

$$\left\{ -\nabla \frac{\hbar^2}{2m_c(\vec{r})} \nabla + V_c(\vec{r}) \right\} F_1 = E F_1 \quad (4)$$

where m_c is the effective mass of the electron and V_c is the band-edge energy. Both m_c and V_c have different but constant values in different materials. They are found either by fitting to experimental data or from *ab-initio* calculations, hence the $k \cdot p$ method is an empirical method. We further note that the parameters are the bulk-like ones.

The multiband $k \cdot p$ method applied to quantum wires is similar to the theory for other nanostructures (quantum wells, quantum dots) except for the different degree of confinement. For nanowires (free-standing) it is customary to use Dirichlet boundary conditions on the surface as the wave function is assumed to be zero outside the structure (infinite barrier). However, in case the plane-wave expansion method is used it is not feasible to use Dirichlet

boundary conditions, instead a large but finite confinement potential is used.¹²⁹ This is consistent with the choice of Maslov and Ning¹³⁰ and Galeriu et al.¹³¹ Especially for the eight-band model, the plane-wave method is preferred because one does not have the problem of spurious solutions which is present using, e.g., the finite-element method.¹³² Also, within the envelope-function formalism, there is a requirement that the plane-wave expansion of the envelope functions should be restricted to the first Brillouin zone, and this is most easily guaranteed using a plane-wave expansion method.

The application of the multiband $k \cdot p$ to free-standing nanowires is still rather rare; most of the calculations have been carried out by only two groups.^{68, 129, 130, 133–136} The work done in Ning's group used the Luttinger-Kohn Hamiltonian while the work of Lassen and coworkers used the Burt-Foreman one. Recently, eight-band models for zincblende semiconductors have been implemented for the nanowires.^{129, 130} As an example, we show in Figure 4 the valence-band dispersion curve of a cylindrical free-standing InAs with a 5 nm diameter.¹²⁹ The difference in band structure between the six-band and eight-band is visible. Maslov and Ning¹³⁰ have also shown the impact of the models on the optical properties.

The standard Hamiltonian for wurtzite materials has been a six-band model for the valence band and a one-band model for the conduction band. The original formulation for bulk valence bands was due to Rashba, Sheka, and Pikus (RSP Hamiltonian),^{137, 138} and the Hamiltonian is quadratic in the wave vector. Application to heterostructures was proposed by Sirenko et al.¹³⁹ and Chuang and Chang¹⁴⁰ using the old symmetrization technique. More recently, Mireles and Ulloa¹⁴¹ have used the Burt-Foreman envelope function representation to

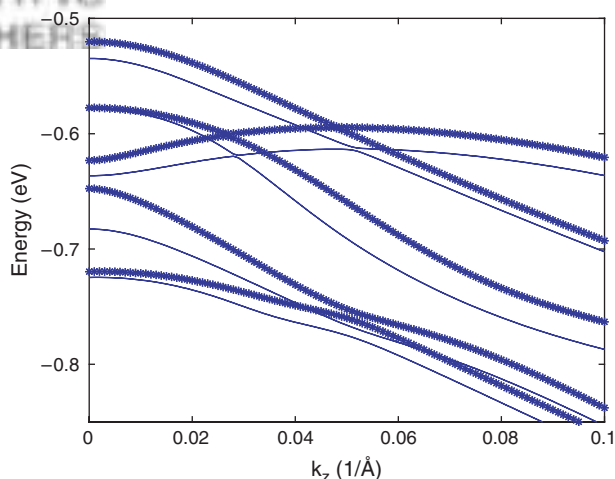


Fig. 4. Band structure of a free-standing cylindrical InAs nanowire with a diameter of 5 nm grown along the [111] direction. The asterisk and solid lines correspond to an eight-band and a six-band calculation, respectively. Reprinted with permission from [129], B. Lassen et al., *J. Mat. Res.* 21, 2927 (2006). © 2006, Materials Research Society.

properly derive the heterostructure Hamiltonian. Another development is the formulation of an analogue of the Sercel-Vahala theory¹⁴² of zincblende semiconductors for wurtzite nanostructures.¹⁴³ This theory is applicable only to nanostructures with axial symmetry. However, this includes cylindrical nanowires and nanorods, and cylindrical and spheroidal quantum dots, among others. For cylindrical nanowires, one can further appeal to periodicity along the wire axis in order to reduce the problem to a one-dimensional one. This new representation of the $k \cdot p$ theory significantly improves the computational requirements for calculating the electronic properties of wurtzite nanowires and nanorods of cylindrical symmetry. Advantages of $k \cdot p$ methods are the ability to treat large structures, and the physical transparency of the model via its input parameters (e.g., effective masses). Disadvantages include inapplicability for very small nanostructures (e.g., <2 nm), lack of self-consistency, and inability to treat atomic relaxation.

3.2. Tight-Binding Method

There have been calculations of nanowire band structures using the empirical tight-binding (TB) method as well. Thus, a few groups have studied zincblende embedded quantum wires in the past,¹⁴⁴ and free-standing nanowires.^{145–156} We are not aware of any papers on wurtzite nanowires; indeed, a search on INSPEC in January 2007 came up empty. Just as for $k \cdot p$ theory, the implementation of the TB theory for nanowires is similar to the theory for other nanostructures (quantum wells, quantum dots) except for the different degree of confinement.

The TB Hamiltonian matrix element is given by

$$\begin{aligned} \langle b, \alpha, \mathbf{k} | H | b', \beta, \mathbf{k} \rangle &= \sum_{\mathbf{R}} e^{i\mathbf{k} \cdot (\mathbf{R} + \boldsymbol{\tau}_{b'} - \boldsymbol{\tau}_b)} \langle \mathbf{0}, b, \alpha | H | \mathbf{R}, b', \beta \rangle \\ &\equiv \sum_{\mathbf{R}} e^{i\mathbf{k} \cdot (\mathbf{R} + \boldsymbol{\tau}_{b'} - \boldsymbol{\tau}_b)} E_{bb'}^{\alpha\beta}(\mathbf{R}) \end{aligned} \quad (5)$$

where \mathbf{R} stands for lattice vectors, b and b' label the atoms in a unit cell, α and β label the atomic orbitals, and $\boldsymbol{\tau}_b$ labels the atomic position within a unit cell. The summation is appropriately carried out in a shell expansion and truncated after a certain number of neighboring interactions. A nanowire allows one to define a periodicity along the wire axis, labeled by the wave vector \mathbf{k} , and thus the size of the Hamiltonian matrix grows with the cross-sectional size of the wire. Due to the local interactions of the model, the resulting matrix is a sparse one of size $\sim N_a \times N_o$, where N_a is the number of atoms in a unit cell and N_o is the number of orbitals per atom. The standard techniques that have been applied are the Lanczos and iterative Jacobi–Davidson algorithms. Thus, it is possible to diagonalize the matrix for the pertinent eigenvalues and eigenvectors. The parameters of the TB theory are: the bulk TB parameters $E_{bb'}^{\alpha\beta}(\mathbf{R})$, and the band offset between

different materials. For a free-standing NW, the dangling bonds at the surface are passivated by using hydrogen atoms^{146, 154} and reconstructions are neglected. Indeed, the surface is typically defined to be made of those atoms exposed when all the atoms outside a certain boundary are removed.¹⁴⁶

At this point, Persson and Xu^{147–149, 153} have only used the nearest-neighbor sp^3s^* Vogl parameters;¹⁵⁷ these are known to lead to unsatisfactory conduction bands (except for the location of the minima). For example, the effective mass of the electron is typically about twice the actual experimental value.¹⁵⁸ Most other recent work,^{152, 154, 155} on the other hand, have used more accurate $sp^3d^5s^*$ parameter sets.

Tight-binding models are less efficient than $k \cdot p$ ones and the TB parameters are less transparent. Yet its main advantages are its atomistic and full Brillouin zone representations. It is, therefore, applicable down to atomic scale and has been used for Si NW's.¹⁴⁵ Furthermore, self-consistency is possible.

3.3. First-Principles Methods

There is a fairly large number of theoretical studies on semiconductor nanowires using first-principles techniques, with the majority of them on Si nanowires,^{146, 156, 159–171} fewer on Ge nanowires,^{168, 172–175} and even less on III–V and II–VI nanowires.^{176–178} Additionally, Si/Ge core-shell nanowires,^{179, 180} GaN/GaP core-shell nanowires,¹⁸¹ and hypothetical atomic chains of group IV, III–V, and II–VI semiconductors¹⁸² have also been studied by first-principles techniques. Continuum approaches (e.g., $k \cdot p$ envelope function in conjunction with elastic theory for strain) are often found to be very useful for obtaining qualitative physical pictures and even quantitative results for relatively large and simple structures. There are a number of situations for which first-principles techniques are expected to be more appropriate, in spite of the fact that they demand significantly more computational resources: (1) It is well known that the $k \cdot p$ envelope-function approach becomes problematic when applied to small nanostructures, say, with a size of 1–2 nm; the neglect of the interfacial nonlocal terms as mentioned above in Section 3.1 becomes ambiguous for the small wires. (2) It is difficult to apply the $k \cdot p$ envelope-function approach to nanostructures based on indirect band-gap materials (e.g., Si), particularly for understanding the selection rule of the interband optical transition. (3) The wire shape is usually closely related to the crystal structure of the host material, and thus the atomistic nature makes the wire surface faceted in different ways depending on the wire orientation. Figure 5 shows an example of a nanowire structure with faceted surface (an [111]-oriented GaN nanowire). For small wires, the atomistic character of the wire shape becomes critically important for determining the electronic structure of the wires. (4) A small wire

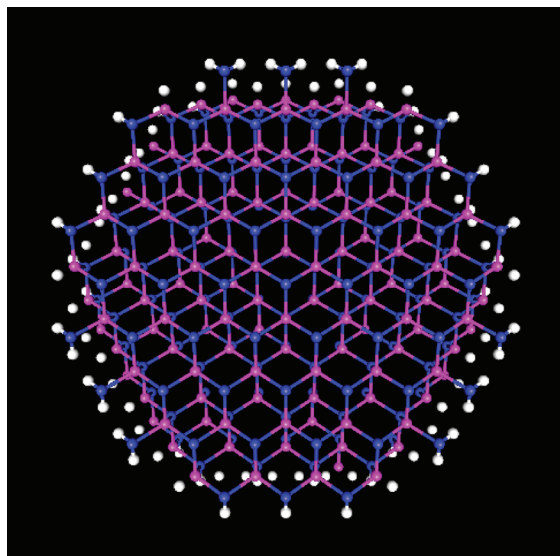


Fig. 5. Top view of a zincblende nanowire with a diameter of 2.3 nm ($2\sqrt{13}/2a$), passivated with pseudo-hydrogen atoms (in white color). The horizontal axis is in the zincblende $[\bar{1}10]$ direction, and the vertical is $[\bar{1}12]$. The facets are $(\bar{1}, \bar{1}, 2)$ -like planes.

might be found to form with a different crystal structure from the bulk, thus, the bulk parameters are not usable for such a wire. (5) The surface states and their passivation are much more feasible to be investigated by a first-principles technique. (6) For complex structures (e.g., axially or radially modulated wires), effects associated with lattice relaxation, band alignment, charge transfer and polarization are rather inconvenient to be treated correctly if not impossible within a continuous model. Additionally, certain needed input material parameters (e.g., band offsets and absolute deformation potentials) for the continuous model are not defined or given free of ambiguity, thus a first-principles technique could in principle avoid these issues. (7) For structures involving experimentally less well studied materials, finding appropriate input parameters for the continuous model is a great challenge. In fact, even empirical atomistic approaches (e.g., empirical pseudopotential) could face some problems similar to those of a continuum model, for instance, the polarization effect, finding the appropriate input parameters like band offsets and absolute deformation potentials. In spite of the advantages that a first-principles approach might have over a continuum model, because of the well-known local density approximation (LDA) typically adopted in any density functional theory (DFT), first-principles approach usually cannot yield an electronic band structure accurate enough to be directly comparable with experimental data. Empirical corrections could be introduced to mitigate the LDA errors in the band gaps, at least to some extent. One of these approaches is to introduce corrections into the non-local pseudopotentials to fix the LDA errors in the band gaps at different critical points of the binary semiconductor¹⁸³ or alternatively the LDA

error in the conduction-band effective mass (LDA+C).¹⁷⁶ Unfortunately, it is not easy to simultaneously get both the energies and effective mass corrected. Another is a beyond-LDA approach (i.e., GW), which is more demanding in computational resources than the LDA approach, but is generally considered to be the most accurate approach for the band structure, and is slowly inching its way into nanostructure modeling. Nevertheless, it is not unusual to see GW results with an error of 100–200 meV in the band-gap energy even for binary semiconductors. Thus, one should not take for granted that a first-principles theory (either within or beyond the LDA) can predict nanowire electronic band structures with the accuracy typically expected by experimentalists and needed for practical applications. It is the general guidance and direction provided by these computations that is often more meaningful than the actual numerical values.

Because of the well-known fact that dangling bonds typically introduce surface states in the band gap, surface passivation is often applied to the nanowires in reality as well as in the first-principles studies of the nanowires. For Si and Ge nanowires, H atoms are probably the most natural species for the passivation both in reality and the theoretical study. For III–V or II–VI nanowires, to preserve local charge neutrality, pseudo-H atoms (with non-unity nuclear charge Z) instead are probably better options for the surface passivation for certain purposes in the theoretical investigation of these nanowires, as has been demonstrated in the electronic-structure modeling of III–V and II–VI quantum dots.^{184, 185} There are basically two motivations for applying passivation species to the nanowires in theoretical studies. The most common motivation is to passivate the surface states of the dangling bonds within the band gap or near the band edges of the fundamental band gap so that the bulk-like states near the fundamental band gap of the pristine nanowire can be conveniently identified and calculated. Ideally, for this purpose, a successful passivation should be able to position the surface states associated with the passivated dangling bonds far away from the both the valence-band maximum (VBM) and conduction-band minimum (CBM). However, finding the optimized passivation (e.g., the appropriate bond lengths between the passivation species and the atoms on the surface) might not be trivial.¹⁸⁶ If the optimization procedure is not appropriately done, the quantitative results (e.g., band gap vs. wire size) could be inadvertently distorted. Additionally, the existence of the surface states somewhere in the conduction or valence band could potentially affect the calculations for the material properties that depend on the global energy spectrum (e.g., dielectric functions). The other motivation for applying the passivation is to actually find out which type of passivation could yield energetically more stable nanowire structures and the corresponding electronic structure. It is expected that the optimized passivation with the latter motivation could be very different from that obtained under the penultimate consideration,

especially for small nanowires the contribution of the surfaces to the total energy could be quite significant. Thus, even for the same interior structure, the two different passivation procedures could potentially yield rather different results, which should be kept in mind when we attempt to compare the results of different publications.

There is a recent quasi-self-consistent implementation of an *ab initio* pseudopotential theory, known as a charge-patching method,¹⁸³ that is allowing larger nanostructures to be modeled. The charge-patching method allows one to obtain nearly the same charge density as would be calculated directly by the self-consistent calculation, and it has been shown to be able to reproduce the eigenstates of the self-consistent calculation with an accuracy of about 10 meV. This method is particularly useful for a large system that is practically impossible to do using the self-consistent calculation. With this technique, the atomistic charge motifs are first obtained from self-consistent calculations of small clusters. For a large system, the charge motifs are assembled to obtain the charge density that is then used to generate the local potential of the system. The obtained local potential of the system and the non-local atomic pseudopotentials can then be used to selectively calculate the electronic states of interest near a given energy reference using a “folded-spectrum method.”¹⁸⁷ Because it is an atomistic method, when applying it to the nanowire problem, one can also examine effects like lattice relaxations, surface states and passivation that are less straightforward to study with the $k \cdot p$ theory.

3.4. Empirical Pseudopotential Methods

Other methods that have been used for computing the electronic structures of nanostructures include the empirical pseudopotential methods that have been fitted to *ab initio* bulk potentials. One of the latest versions is the so-called semiempirical pseudopotential method (SEPM) or screened atomic potential (SAP). It has been used by Li and Wang¹⁷⁶ and Karanth and Fu¹⁷⁸ for nanowires of few materials, because of the limited availability of such pseudopotentials. However, currently published results were restricted to sizes less than 5 nm.

4. ELECTRONIC PROPERTIES

Both quantum wires and nanowires have a one-dimensional band structure (see, e.g., Fig. 4). There is much to characterize in this plethora of curves (symmetry, crossing, extrema, ...) and we will discuss a few of those below. Nevertheless, the main focus in the present article will be on the size and shape dependence of the fundamental band gap and of the effective masses.

4.1. Quantum Wires

Since quantum wires were studied before nanowires, we very briefly review some of the results on the former. One

of the earliest applications of $k \cdot p$ for the conduction-band states of quantum wires using pseudopotentials by Jaros' group in 1987 on GaAs/AlGaAs QWR's.¹⁸⁸ The first calculation on valence subbands was by Brum et al. in 1987¹⁸⁹ within a four-band spherical approximation. Citrin and Chang in 1989¹⁹⁰ applied the six-band $k \cdot p$ to rectangular GaAs/Al_{0.2}Ga_{0.8}As QWR's. One result of the latter is that crossing behaviour of the first two VB in a square QWR (due to Γ_6 and Γ_7 symmetries of C_{4v}) becomes anti-crossing in a rectangular QWR (due to all states being Γ_5 of C_{2v}). This might be the first report of crossing in the top of the VB for a QWR. Another result is the mixing of HH and LH even at $k = 0$. Typical cross-sections were 10 nm by 10 nm. Sercel and Vahala^{142, 191, 192} studied cylindrical GaAs/Al_{0.3}Ga_{0.7}As QWR's with both infinite and finite barriers using a four-band model within the axial approximation; this led to the introduction of a quantum number F_z . They went down to 2 nm diameter in their calculations though one might question the applicability of $k \cdot p$ at that point; the largest diameter considered was 20 nm. In k_z -space, their results for the $d = 5$ and 5 nm QWR's show that the $F_z = 1/2$ state is lowest in energy at $k_z = 0$ but the $F_z = 3/2$ is lower at finite k_z (though Sercel and Vahala did not explicitly refer to this); this is, in fact, the crossing reported by Citrin and Chang. For $d = 10$ nm, the first two states at $k_z = 0$ both have $F_z = 1/2$ and they have opposite envelope parity, but for $d = 5$ nm, the first two states at $k_z = 0$ are the even $F_z = 1/2$ and $F_z = 3/2$ states.^{142, 192} The transition appears to occur around $d = 6$ nm. However, in another paper,¹⁹¹ they report, for a 10 nm QWR, that the first two states at $k_z = 0$ both have even parity, the lowest only has 30% HH, the next one has 68% HH component. We believe the discrepancy is due to the use of an infinite barrier in the latter case. Finally, as the diameter is increased, the lowest two states approach each other to within 5 meV for $d = 20$ nm but no crossing appears at $k_z = 0$. A few more recent papers have appeared though we will not focus on these work.^{193, 194}

For applications to V-groove QWR's, almost all of the work have been restricted to one-band models for both the conduction and valence states.^{195–199} Chang and Xia,¹⁹⁵ and Sun¹⁹⁶ studied the quantum-confined Stark effect; Chang and Xia, and Deng et al.¹⁹⁷ looked at excitons; and, finally, Chang and Xia used an idealized faceted wire geometry, while Sun and Deng et al. used analytical smooth profiles. One exception to the above simplified calculations is the work of Siarkos and Runge²⁰⁰ where they treated the valence band using the Luttinger–Kohn Hamiltonian, used a realistic wire geometry, and calculated the full exciton dispersion.

It is worth mentioning that the work using the $k \cdot p$ approach on QWR's is mostly focused on the nearly lattice matched system GaAs/AlGaAs. When strain, especially inhomogeneous strain, is present, the $k \cdot p$ method becomes rather complicated and cumbersome, for instance, when applied to certain embedded QWR's.²⁰¹

4.2. Nanowires

There are a few theoretical studies of the size dependence of the band gap^{33, 45, 129, 152, 154, 173, 176, 178} in addition to experimental data.^{33, 38, 45, 52, 53, 57, 202} We have found few papers on the band structure of wurtzite nanowires using $k \cdot p$ and none using TB. One of the earliest appears to be work on ZnS nanowires,⁶⁸ though a calculation for GaN nanowires has now been published.¹³⁶

In a one-band $k \cdot p$ model with infinite potential barrier, the confinement energy should scale as d^{-2} . That the scaling is different when a finite barrier is taken into account was already found by Delley and Steigmeier.¹⁶⁴ In their studies on (100) Si NW's, they actually obtained a linear dependence using an effective-mass model. Other reasons for a deviation from the inverse-square law include a multiband theory,¹³⁰ excitonic corrections,⁴⁵ and self-energy corrections.¹⁵⁴ There are also studies of the ratio of the confinement energies of wires and dots,^{53, 176} however, since that relies on the validity of the inverse-square scaling rule and on comparing to quantum dots, we refer the reader to the two citations provided for a discussion.

One of the earliest models of the size-dependent energy assumed the corresponding effective-mass result with inclusion of excitonic correction that was originally derived for microcrystallites:^{45, 203}

$$\Delta E_g = \frac{2\pi^2 \hbar^2}{d^2} \left[\frac{1}{m_c} + \frac{1}{m_h} \right] - \frac{3.6e^2}{\epsilon_\infty d} \quad (6)$$

where m_c (m_h) is the electron (hole) effective mass, and d is the wire thickness (diameter for a cylindrical shape or a related size measure for other shapes). For example, Read et al. defines¹⁶⁰

$$d = a_0(2M)^{1/2}/4 \quad (7)$$

where M is the number of atoms per unit cell and a_0 is the lattice constant. Note that, in addition to using a quantum dot result for a NW, previous applications have also used the bulk effective masses.^{33, 45}

More accurate calculations have obtained numerical results for the band gap. One can then curve fit the band gap and the effective mass according to the following expressions:¹²⁹

$$\Delta E_g = b_g \cdot d^{-n_g} \quad (8)$$

$$m^* = a_m + b_m \cdot d^{-n_m} \quad (9)$$

On the other hand, Niquet et al.^{154, 204} fitted the band-edge energies to

$$E(d) - E(\infty) = \frac{K}{d^2/4 + ad/2 + b} \quad (10)$$

The rationale is to reduce the excessive confinement displayed by an infinite-barrier effective-mass model by a linear term for small radii. A parametrization that accounts for the wire length was given by Yorikawa et al.¹⁴⁶

$$\Delta E_g = \frac{\alpha}{(d/2a_0)^n} \left[1 + \beta e^{-\gamma 2L/d} \right] \quad (11)$$

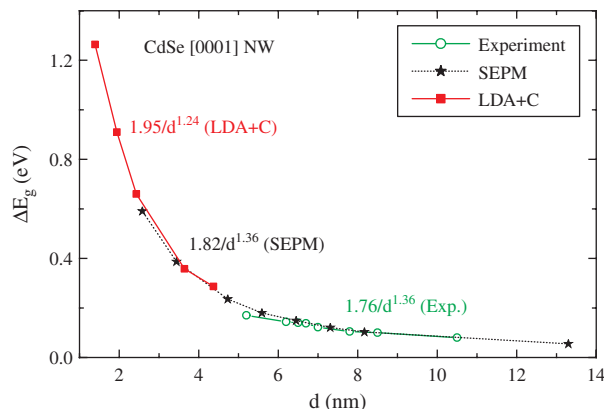


Fig. 6. Confinement energy obtained using an *ab initio* (LDA+C) calculation compared to semi-empirical pseudopotential method (SEPM) and experiments on CdSe nanowires.³⁸ Adapted with permission from [176], J. Li and L.-W. Wang, *Phys. Rev. B* 72, 125325 (2005). © 2005, American Physical Society.

where a_0 is the bulk lattice constant and L the length of the wire.

Li and Wang¹⁷⁶ did an extensive first-principles study (using the charge-patching method) of the size dependence of the band gap for nanowires of: CdSe, CdS, CdTe, InP, GaAs, InAs, ZnS, ZnSe, ZnTe, ZnO, GaN, InN, and AlN. Zincblende (wurtzite) nanowires are oriented along [111] ([0001]) with a hexagonal cross section. Dangling bonds are passivated with pseudoatoms as described earlier. As an example, their results for CdSe are reproduced in Figure 6 where they are also compared to experimental data. We note that they extended the range of the wire size by using the SEPM for CdSe and InP. It is clear from Figure 6 that a single index in the power law cannot fit the band-gap scaling data over a wide range of cross-sectional dimensions. The general agreement appears good though we note that the calculations do not include excitonic and dielectric-mismatch corrections. Data they obtained for other materials are reproduced in Figure 7. There are few other results to compare the latter to. One could note, for example, that our calculation of quantum-confinement energy for [0001] ZnS is around 160 meV for a 5 nm wire⁶⁸ and Li and Wang obtained about 190 meV. Such a difference is not atypical of different methods. Another comprehensive work is a TB calculation by Niquet et al.¹⁵⁴ for: Si, Ge, InAs, GaAs, InP, GaP. They did calculations for [001], [110] and [111] growth directions (additionally [112] for Si) and with cylindrical shapes. The two works are compared in Figure 8 for GaAs and InAs. Overall, there is semi-quantitative agreement between those two calculations.

There are a few calculations of the shape dependence of the band structure.^{129, 134, 153, 156} An example for a GaAs/AlGaAs quantum wire is shown in Figure 9. It can be seen that the differences in the top valence bands are small except for a change in crossing/anticrossing behaviour as a result of symmetry change. Luisier et al.¹⁵⁶ had reported a

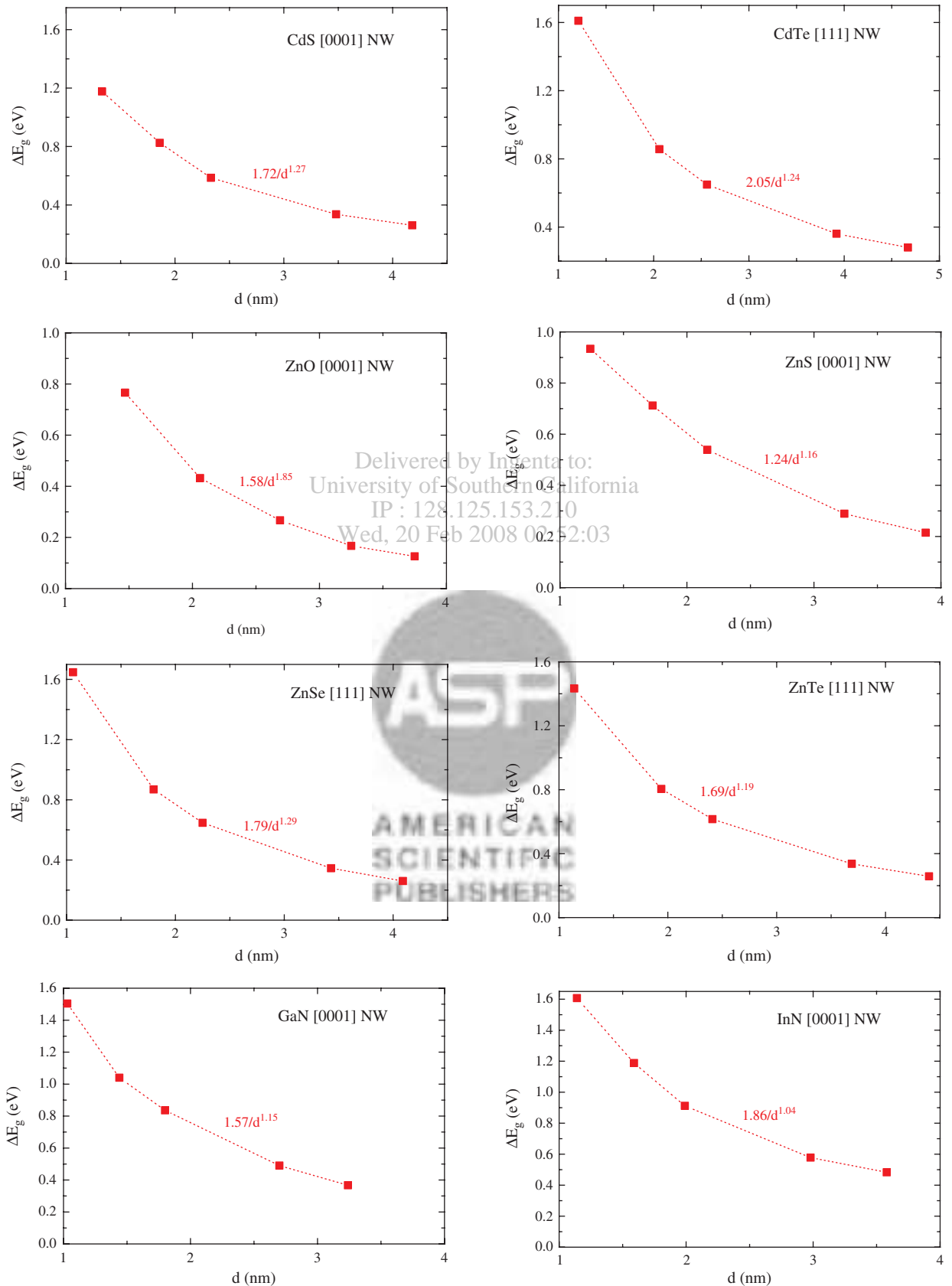


Fig. 7. Confinement energy obtained using an LDA+C calculation for CdS, CdTe, ZnO, ZnS, ZnSe, ZnTe, GaN, InN, and AlN nanowires. Reprinted with permission from [176], J. Li and L.-W. Wang, *Phys. Rev. B* 72, 125325 (2005). © 2005, American Physical Society.

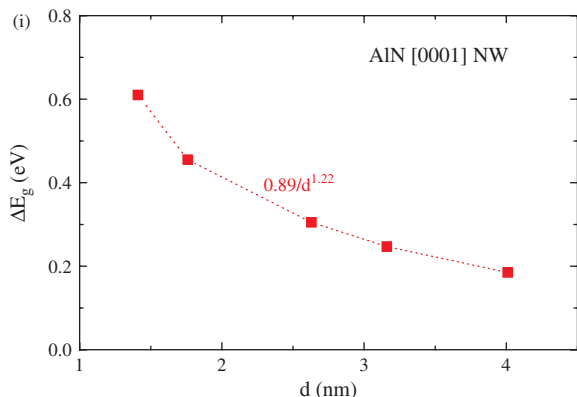


Fig. 7. Continued.

substantially bigger change for Si nanowires. However, we believe the origin of that is due to the cross-sectional area changing from one shape to another. This is corroborated by the change in the confinement energy at the zone center.

Various data sets are given in Tables II–III for the fitted parameters. There are fewer calculations of the effective masses of carriers in nanowires.^{129, 154, 178} Examples are given in Table IV.

We now review the literature for a few materials.

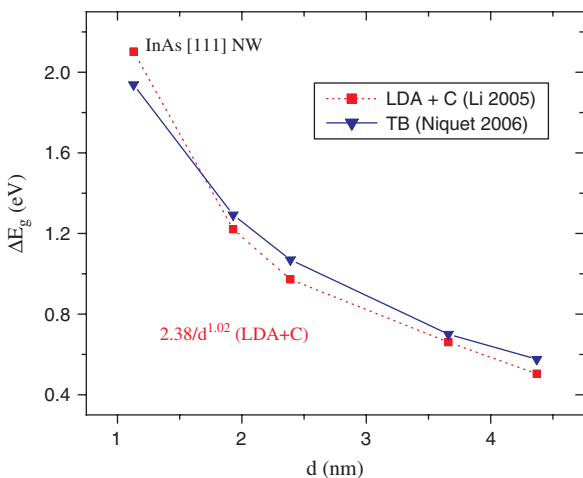
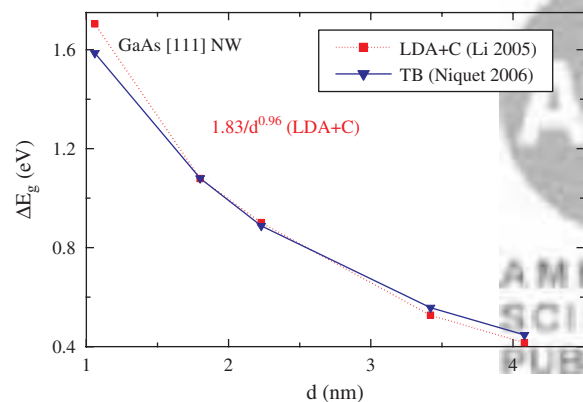


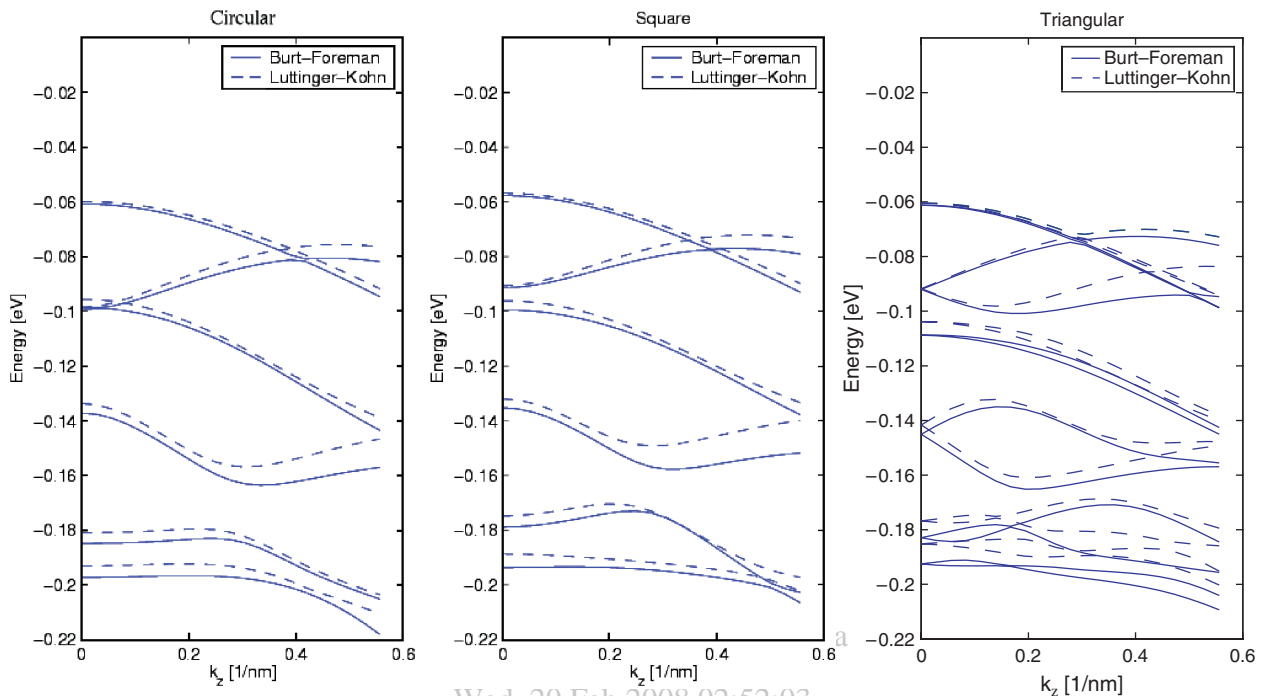
Fig. 8. Confinement energy obtained using an LDA+C¹⁷⁶ and a TB¹⁵⁴ calculation for [111] GaAs and InAs nanowires.

4.2.1. Si and Ge Nanowires

The electronic properties of Si and Ge nanowires have so far mostly been studied using *ab initio* techniques,^{159–171, 205–208} with a few TB calculations.^{146, 150, 152, 154, 156, 204} Interest in Si is due to the fact that Si NW's were postulated to be at the origin of the blue-shifted strong luminescence in porous Si. For Si nanowires, most studies have assumed the wire surfaces to be simply truncated ones of the bulk crystals, although they could be either passivated or not by H atoms, except for few cases where reconstructed surfaces,^{167, 209} or even interior structures different from the bulk Si have been considered.^{206, 210} Here we will focus on the studies that have assumed the nanowires preserving the bulk-like interior structure.

Early efforts focused on the [001] oriented wires with relatively small sizes but with H passivation.^{159–165} The key findings included direct band gaps, a large band-gap blue shift, and the optical anisotropy between the longitudinal and transverse direction of the wire. The direct gap and the order of energy levels at the Γ point were explained in terms of the folding effect of the six conduction band minima at $(0.085, 0, 0)k_0$, $(0, 0.085, 0)k_0$, and $(0, 0, 0.085)k_0$.^{159, 162} Because the longitudinal effective mass m_l is much greater than the transverse m_t , the first four in-plane minima that have large average effective mass of the longitudinal and transverse directions give rise to four lower subbands, and the other two minima of which only the transverse direction are subjected to the quantum confinement yield two higher subbands. Although the nanowire was consistently found to be direct band gap, the interband dipole transition matrix element was found to be very small at the band gap,^{159, 161, 163} but it was indicated that the excitonic effect could significantly enhance the oscillator strength.¹⁶² For the weak optical transition at the band gap, Read et al.¹⁵⁹ and Saitta et al.¹⁶⁵ have found that the matrix element for the z polarization (i.e., parallel to the wire axis) is much greater than those for the x and y , whereas Ohno et al.¹⁶² and Hybertsen and Needels¹⁶³ have indicated that the opposite case is true. Delley and Steigmeier¹⁶⁴ have suggested that the effect of H passivation might be considered as a model wide-gap material where the bonding and anti-bonding Si–H states define the effective barrier heights for the hole and electron, respectively. Hybertsen and Needels¹⁶³ have further pointed out that because the Si–H states are usually resonant, Si–H character is expected to spread over the entire spectral range.

Filonov et al.²⁰⁵ and more recent studies have extended to Si nanowires of other orientations, including [110], [111], and [112] as well as larger sizes.^{152, 154, 166–168, 170} For the nanowires of comparable sizes and passivated by H atoms but without surface reconstruction, the general trend for the band-gap blue shift is found to be $\Delta E_g[100] > \Delta E_g[111] > \Delta E_g[112] > \Delta E_g[110]$,^{166, 168, 170} although the



Wed, 20 Feb 2008 02:52:03

Fig. 9. Band structure of [001] GaAs/AlGaAs quantum wires of same cross-sectional area. Reprinted with permission from [134], B. Lassen et al., *Solid State Commun.* 132, 141 (2004). © 2004, Elsevier B.V.

early work of Saitta et al.¹⁶⁵ had indicated the shifts are practically the same for the [100] and [111] wires, while the more recent work of Harris and O'Reilly gives $\Delta E_g[100] > \Delta E_g[111] \approx \Delta E_g[110]$. Zhao et al.¹⁶⁶ have investigated unrelaxed nanowires with size up to 4 nm, and shown that the [110] wire exhibits a direct gap, as a result of the projection of the two CBM's at $(0, 0, 0.085)k_0$ onto the Γ point, but the [111] wire instead to have an indirect gap, unless the wire diameter $d < 2$ nm then it becomes direct. Both Zhao et al.¹⁶⁶ and Li and Freeman¹⁶⁹ have shown the direct band gap to be optically inactive for either the [110] wires or the [111] and [100] wires, i.e., the transition matrix elements are "vanishingly small near the bandgap."¹⁶⁶ The appearance of the optically inactive direct band gap has been pointed out not to be due to the symmetry selection rule rather than to be the results of "quantum-confinement effects."¹⁷⁰ For the dielectric function of the nanowire, Zhao et al.¹⁶⁶ have surprisingly found that the optical anisotropy diminishes quickly with d as small as 2 nm. However, Bruneval et al.²⁰⁸ have pointed out that the diminished anisotropy is caused by neglecting the so-called depolarization or local-field effects that may suppress the absorption at the lower energies for the light polarization perpendicular to the wire and, thus, if included, the anisotropy remains strong. Since the local-field effects are quite sensitive to the wire spacing, they might contribute to the controversy on the anisotropy of the band-edge transition found in the early first-principles calculations for the [001] nanowires.^{159, 162, 163}

For examining the scaling rule of ΔE_g versus d , a size-independent self-energy correction was typically assumed.^{159–162} However, it has been noted that the LDA errors could be quite different between SiH_4 and Si ¹⁶³ or between SiH_2 and Si ,¹⁷⁰ thus, some sort of weight averages have been suggested for correcting the LDA errors for the H-passivated Si nanowires. Direct GW calculations of Zhao et al.¹⁶⁶ have shown that the GW correction sensitively depends on the wire size. In general, the scaling rule ΔE_g versus d , being nearly linear for small wires, is found to be quite different from that predicted by a simple "particle-in-a-box" model, $\Delta E_g \propto d^{-2}$.^{159–161, 164, 166} The results of Delley and Steigmeier¹⁶⁴ was recently shown to be very similar to a TB calculation¹⁵⁴ (Fig. 10). Indeed, there was general agreement between TB and LDA calculations for [001] and [111] nanowires. The LDA calculation of Read et al.^{159, 160} is included even though the NW is slightly rectangular. Comparison between theory and scanning tunneling spectroscopy (STS) for [001] NW's was less successful,¹⁰⁹ with the theory underestimating the gap (by almost 1 eV!) for small nanowires.¹⁵⁴ Nevertheless, the single experimental point for a [110] NW agrees perfectly with the TB results; note also the much larger confinement energies obtained using a GW calculation.¹⁶⁶ Hence, it has been argued that maybe the experimentally-determined sizes are incorrect for very small wires.¹⁵⁴ The older TB calculation of Yorikawa et al.¹⁴⁶ appears to underestimate the gap (Fig. 10).

The effects of atomic relaxation have been examined. Buda et al.¹⁶¹ have indicated that the relaxation causes an

Table II. Fitted parameters describing the size dependence of the band gap of nanowires.

Material	Orientation	K (eV nm ²)	a (nm)	b (nm ²)	
Si	[001]	$v = -0.8825$	$v = 1.245$	$v = 0.488$	
		$c = 0.6589$	$c = 0.235$	$c = 0.142$	
	[110]	$v = -0.6825$	$v = 2.062$	$v = 0.996$	
		$c = 0.6470$	$c = 0.123$	$c = 0.849$	
	[112]	$v = -0.7075$	$v = 2.616$	$v = -0.083$	
		$c = 0.7273$	$c = 0.246$	$c = 0.313$	
	[111]	$v = -0.6964$	$v = 3.664$	$v = -0.374$	
		$c = 0.8010$	$c = 0.342$	$c = 0.212$	
	Ge	[001]	$v = -1.8294$	$v = 2.938$	$v = 0.159$
			$c = 1.8505$	$c = 0.930$	$c = 0.640$
		[110]	$v = -1.6159$	$v = 4.310$	$v = 0.579$
			$c = 1.3299$	$c = 0.825$	$c = 0.873$
[111]		$v = -1.5720$	$v = 5.007$	$v = 0.640$	
		$c = 1.5161$	$c = 0.746$	$c = 0.717$	
InAs	[001]	$v = -1.2243$	$v = 2.181$	$v = 0.583$	
		$c = 10.6948$	$c = 6.512$	$c = 2.406$	
	[110]	$v = -1.0051$	$v = 2.548$	$v = 1.379$	
		$c = 10.5845$	$c = 6.645$	$c = 2.879$	
	[111]	$v = -0.9887$	$v = 2.720$	$v = 0.898$	
		$c = 10.6951$	$c = 6.512$	$c = 2.773$	
GaAs	[001]	$v = -1.0320$	$v = 2.026$	$v = 0.401$	
		$c = 3.4198$	$c = 1.786$	$c = 1.103$	
	[110]	$v = -0.8035$	$v = 2.608$	$v = 1.079$	
		$c = 3.3448$	$c = 1.615$	$c = 1.915$	
	[111]	$v = -0.8678$	$v = 2.731$	$v = 0.935$	
		$c = 3.4098$	$c = 1.806$	$c = 1.467$	
InP	[001]	$v = -0.9179$	$v = 2.058$	$v = 0.008$	
		$c = 3.0422$	$c = 1.620$	$c = 1.144$	
	[110]	$v = -0.8109$	$v = 3.327$	$v = 1.148$	
		$c = 3.0365$	$c = 1.170$	$c = 1.460$	
	[111]	$v = -0.8273$	$v = 4.465$	$v = 0.223$	
		$c = 3.0696$	$c = 1.798$	$c = 1.214$	
GaP	[001]	$v = -0.8314$	$v = 1.469$	$v = 0.126$	
		$c = 0.3780$	$c = -0.397$	$c = 0.287$	
	[110]	$v = -0.6794$	$v = 2.203$	$v = 1.669$	
		$c = 0.3810$	$c = -0.203$	$c = 0.486$	
	[111]	$v = -0.6942$	$v = 3.557$	$v = 0.287$	
		$c = 0.5589$	$c = 0.000$	$c = 0.285$	

Source: Reprinted with permission from [154], Y. M. Niquet et al., *Phys. Rev. B* 73, 165319 (2006). © 2006, American Physical Society.

overall expansion that approximately follows an r^2 law where r is the distance of the atom from the wire center. Hybertsen and Needels¹⁶³ have found that the relaxation results in a change in the order of the energy levels for the two conduction band states. Note that the relaxation not only changes the Si—Si bond lengths but also the Si—H bonds, and thus the passivation. Li and Freeman¹⁶⁹ have found the relaxed structures have larger band gaps than the unrelaxed ones, but the effect is more significant for the [100] wire than the [111] wire (0.2 eV vs. 3 meV shift for a 1 nm wire). We would like to emphasize that one does need to pay attention to the possible consequences of the variations in Si—H bond lengths and orientations on the band-gap energy, when comparing the different results in the literature. It is evident that even

Table III. Fitted parameters describing the size dependence of the band gap of nanowires.

Material	Orientation	Size (nm)	b_g (eV nm ^{<i>n</i>})	n_g	Reference	
Si	[001]		3.98	1.4	[57]	
CdS	[0001]	1–5	1.72	1.27	[176]	
CdSe	[0001]	1–5	1.95	1.24	[176]	
		[111]	1–5	1.84	1.33	[176]
CdTe	[111]	1–5	2.05	1.24	[176]	
ZnO	[0001]	1.5–4	1.58	1.85	[176]	
ZnS	[0001]	1–4	1.24	1.16	[176]	
ZnSe	[111]	1–4.5	1.79	1.29	[176]	
ZnTe	[111]	1–4.5	1.69	1.19	[176]	
AlN	[0001]	1–4	0.89	1.22	[176]	
GaN	[0001]	1–3.5	1.57	1.15	[176]	
GaAs	[111]	1–4	1.83	0.96	[176]	
		[001]	5–10	5.56	1.47	[129]
InAs	[110]	5–10	5.01	1.44	[129]	
		1–4	2.38	1.02	[176]	
		5–10	5.00	1.45	[129]	
InN	[0001]	1–4	1.86	1.04	[176]	
InP	[001]	5–10	6.61	1.77	[129]	
		[110]	5–10	6.19	1.75	[129]
		[111]	1–4	2.0	1.16	[176]
		2.5–9	2.11	1.36	[176]	
		5–10	5.92	1.75	[129]	

for unrelaxed structures different Si—H bond lengths have been used in different calculations.

A recent work of Vo et al. has specifically searched for energetically favorable hydrogenated Si nanowires.¹⁶⁷ They have found that the structures with symmetrical Si—H bonds (typically adopted in the unrelaxed structures) are less stable than canted Si—H bonds, and the most stable structures are in fact those with surface reconstructions. Although even for the canted wires, the general trend $\Delta E_g[100] > \Delta E_g[111] > \Delta E_g[110]$ remains the same as that for the symmetric wires, the order could change for the reconstructed wires. The direct to indirect switch has been found to depend on both the orientation and surface structure: the bandgap remains direct for canted [001] and [011] wires up to 3 nm in diameter, but becomes indirect for canted [111] wire below 2 nm, although it is still direct for a reconstructed wire. It has been found that the reconstructed wires could have very different band-edge states (e.g., the surface confined states) from those without the reconstruction. The electron and hole effective masses have been calculated for the canted and reconstructed wires, which often exhibit non-monotonic dependence on the wire size. We feel that the variation could reflect non-trivial effects of H passivation. It is interesting to note that all the H-passivated [001] Si nanowires have been consistently found to be semiconductors while Rurali and Lorente have indicated that bare [001] nanowires with reconstructed surfaces are either metallic or semimetallic.²¹¹

All of the above work used H-passivation. A study of the impact of different chemical passivation using DFT (the VASP code) was recently published.¹⁷¹ They specifically looked at the —H, —OH, and —NH₂ groups on small

Table IV. Effective masses of nanowires. Values of a_m , b_m , n_m are fitting parameters for Eq. (9).

Material	Orientation	Size d (nm)	CB (m_0)	VB (m_0)	Reference
Si	[111]	≥ 4	0.4	0.15	[154]
		~ 1	0.62	0.2	[154]
		1	0.64	0.30	[169]
Ge	[001]	1	0.42	1.52	[169]
	[001]		0.55		[154]
	[110]		0.08		[154]
	[111]	1–10		0.07–0.1	[154]
InP	[001]	5–50	$a_m = 0.0795, b_m = 0.617, n_m = 1.75$		[129]
		1–5		1.6–0.4	[178]
	[110]	5–50	$a_m = 0.0795, b_m = 0.445, n_m = 1.71$		[129]
		1–5	0.1–1	0.3–0.2	[178]
	[111]	5–50	$a_m = 0.0795, b_m = 0.385, n_m = 1.70$		[129]
		1–5		0.3–0.2	[178]
InAs	[001]	5–50	$a_m = 0.026, b_m = 0.810, n_m = 1.54$		[129]
	[110]	5–50	$a_m = 0.026, b_m = 0.562, n_m = 1.46$		[129]
	[111]	5–50	$a_m = 0.026, b_m = 0.509, n_m = 1.43$		[129]

(~ 1 nm) [001] Si NW's. They found that the band gap for all passivations are redshifted with respect to the hydrogen one, up to 1 eV. There is thus clearly a dependence of the band gap on the passivation.

One of the few papers to explicitly consider the dielectric-mismatch explicitly and atomistically is a TB calculation using the $sp^3d^5s^*$ model and treating surface passivation by increasing the dangling-bond energy.¹⁵⁶ They calculated the self-energy correction arising from the dielectric discontinuity and found that it should be included when $\epsilon_{in} \gg \epsilon_{out}$ and decrease like $1/d$.

For Ge nanowires, following the same folding argument used for the Si nanowires,^{159, 162} [110] Ge nanowires are expected to have direct band gaps, because the Ge conduction band minima locate at the L points (there are four of them), and two of them are in the plane perpendicular to the wire axis. Indeed, the [110] wires have been found to have direct bandgaps,^{152, 154, 168, 172, 175, 212} whereas the [001] and [111] nanowires have been found to be indirect according to Kholod et al.¹⁷² and Bruno et al.,²¹² but direct for the wire size ~ 1 nm according to Jing et al.,¹⁶⁸ although the energy difference between the direct and indirect gaps is found to be small. In addition, Jing et al. have found that the [112] nanowires remain indirect for the size as small as 0.4 nm. In fact, the order of the direct and indirect band gaps depends on a number of computational details. Nevertheless, the magnitude of the band-gap blue shift seems to follow the same orientation dependence as found for the Si nanowires, that is, $\Delta E_g[100] > \Delta E_g[111] > \Delta E_g[112] > E_g[110]$.^{152, 168, 172, 212} Bruno et al.²¹² have made a connection between such orientation dependence and the geometrical connectivity of the atoms in the wire direction: the [111] and [100] wires appear as a collection of small clusters connected along the axis, while the [110] wires resemble linear chains parallel to the axis. They have made a few additional observations: (1) the GW self-energy corrections are

not only wire-size dependent but also wire-orientational dependent; (2) the exciton binding energy could be large enough to partially cancel the blue shift of the quantum-confinement effect (e.g., for a 0.8 nm [001] wire, the exciton binding = 0.8 eV); (3) the local-field effect diminishes the absorption of the transverse polarization, as it does for Si nanowires;²⁰⁸ (4) the excitonic effect causes a blue shift of the absorption spectrum (a puzzling counterintuitive finding); and (5) structural relaxation results in a small transverse but no longitudinal expansion, and only minor effects on the band structure and optical spectra. However, Jing et al. have indicated that the longitudinal relaxation is actually non-negligible (0.2–1.0%, depending on the wire orientation). If the exciton binding energy is indeed as large as computed by Bruno et al., the selection rule based on the interband transition matrix elements at the Γ point as well as the dielectric functions based on the single-particle theory becomes less practically useful when attempting to explain the experimental data, because the excitonic effects could significantly affect these properties. For certain extreme situations, the single-particle selection rule at the Γ point could even be irrelevant for the experimental situation is typically dictated by the excitonic transition.²¹³

For certain practical applications, the information about band alignments or the shifts of the individual band edges of CBM and VBM is of great importance. However, such information is not readily available in a typical first-principles calculation. To obtain the relative band alignments among different wires, Beckman et al. have used the energy level of a H_2 molecule that is placed at the edge of the supercell as the reference.¹⁷⁵ For Ge nanowires with diameters greater than 1.4 nm, the band-gap change is almost entirely due to the confinement in the conduction band. The scaling law of ΔE_g versus d^{-n_g} seems to vary significantly from one study to the other: $n_g = 0.98$,¹⁷⁵ to

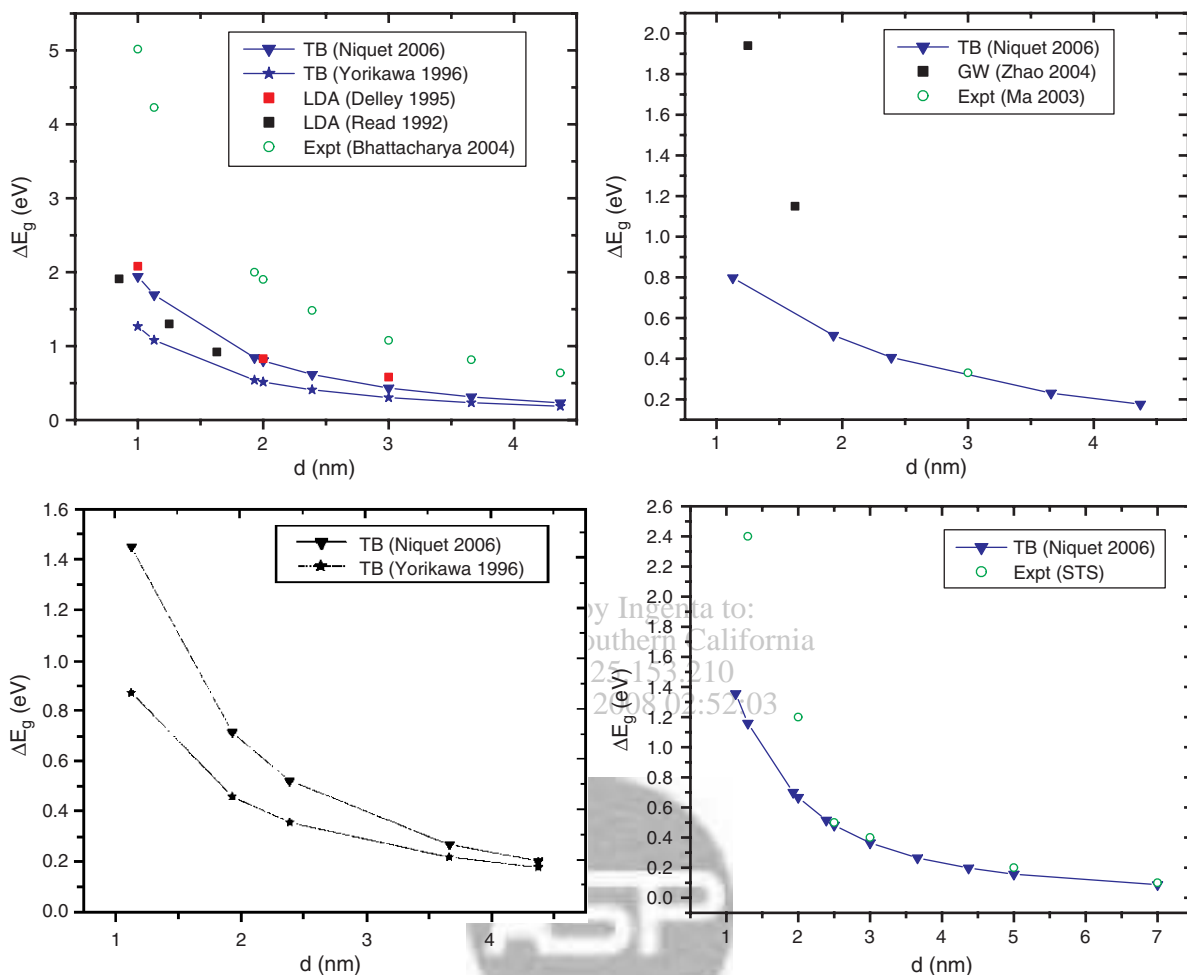


Fig. 10. Confinement energy for cylindrical [001] (top left), [110] (top right), [111] (bottom left) and [112] (bottom right) Si nanowires.

$n_g = 1.7$,²¹² and to not be able to be described by a single exponent.¹⁶⁸ Apparently, the scaling law is affected by a number of factors: for instance with and without the GW correction, with and without including the exciton binding energy, and the details of the passivation. Jing et al. have also tested the passivation with a different molecule (ethine, C_2H). They have found that the overall band structures of the nanowires have changed significantly, and the ethine-passivated structures are more stable than the H-passivated ones.¹⁶⁸

Finally, we have mentioned the difficulty in applying the $k \cdot p$ method to indirect-gap materials. Nevertheless, simple effective-mass-like fit to the quantum-confinement energy has been attempted,¹⁵² and is claimed to work well for Si (Ge) NW's down to about 2–3 (5) nm.

4.2.2. InP

The prototypical III–V material that has received much attention is InP; hence, we include a detailed comparison of the main results on the electronic properties (Table V). All except one of the work on InP assumed a cubic structure. We note, however, that Akiyama et al.¹⁷⁴ obtained the

wurtzite structure as the stable one for diameters less than 2.3 nm if the NW is bare, i.e., not saturated by atoms such as H atoms as was done by others.^{173, 176, 178}

A comparison of the confinement energy obtained using a TB¹⁵⁴ and a $k \cdot p$ ¹²⁹ calculation for [001], [110] and [111] InP nanowires is shown in Figure 11. Since Niquet et al.¹⁵⁴ used a cylindrical cross section, we show a similar $k \cdot p$ comparison even though Lassen et al.¹²⁹ have also studied a hexagonal shape. One notes the surprisingly good agreement between the two independent calculations; the fitting domain was slightly different though

Table V. Experimental and theoretical results on the size dependence of the band gap of [111] InP nanowires.

Method	Size d (nm)	n_g	Comments
<i>Ab initio</i>	1.32–2.13	2	Fails for $d = 1.32$ nm [173]
	1–4	1.16	[176]
SEPM	2–9	1.36	[176]
SAP	1–5	$c = 1.20, v = 2.87$	[178]
TB	2–40	$\frac{K}{d^2/2 + ad/2 + b}$	[154]
$k \cdot p$	5–50	1.75	[129]
Expt	10–50		[52]

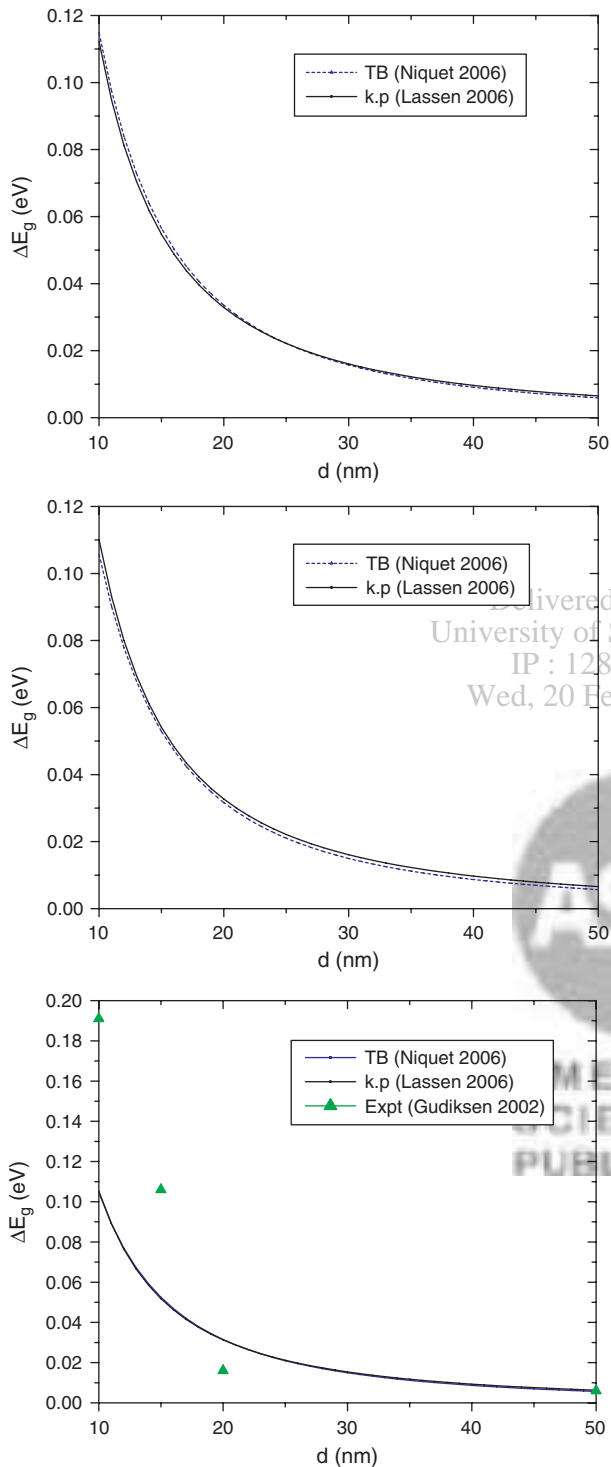


Fig. 11. Confinement energy obtained using TB¹⁵⁴ and a $k \cdot p$ ¹²⁹ calculation for [001] (top), [110] (middle) and [111] (bottom) cylindrical InP nanowires. Experimental data for [111] is from Gudiksen et al. Reprinted with permission from [52], M. S. Gudiksen et al., *J. Phys. Chem. B* 106, 4036 (2002). © 2002, American Chemical Society.

they overlap for 5–20 nm. On the other hand, there are differences between both theories and the experimental data at room temperature⁵² for small diameters. For the experimental data, we used a bulk band gap of 1.35 eV.

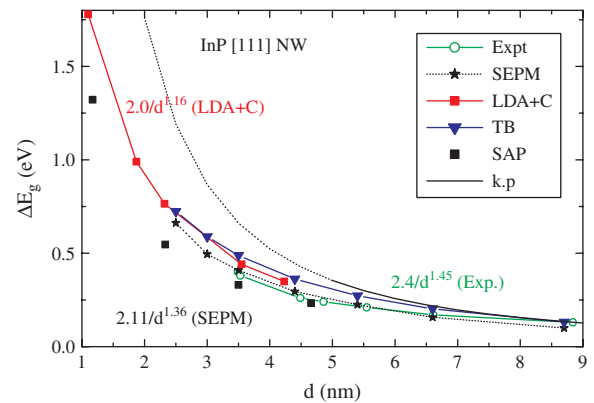


Fig. 12. Confinement energy obtained using a TB,¹⁵⁴ $k \cdot p$,¹²⁹ LDA+C,¹⁷⁶ SEPM¹⁷⁶ and SAP¹⁷⁸ calculations for [111] InP nanowires. Experimental data is from Yu et al. Reprinted with permission from [53], H. Yu et al., *Nat. Mater.* 2, 517 (2003). © 2003, Nature Publishing Group.

Excitonic corrections neglected in the calculations would increase the disagreement with the experiment. Thus, we believe that the experimental blue shifts for small wires ($d < 15$ nm) are likely to be too large. The reason remains to be identified. There are *ab initio*, SEPM/SAP calculations for much smaller nanowires (1–9 nm);^{176, 178} we reproduce their data in Figure 12 with the inclusion of the TB and $k \cdot p$ results. Since $k \cdot p$ was fitted to sizes larger than 5 nm, we include an extrapolation to less than 5 nm as a dotted curve. The latter does display the characteristic overestimate of the confinement energy at that length scale; indeed, the confinement energy at 1 nm is around 6 eV. Overall, all the methods agree well with each other and with the available experimental data between 5 and 9 nm. The TB data agrees with LDA+C ones over the whole domain. However, the recent SAP data¹⁷⁸ appears to underestimate the confinement energy. Other work^{130, 153} did not report the size dependence. We do note that the result of Maslov and Ning for a 6 nm diameter nanowire is over 100 meV smaller than that reported by Lassen et al.;¹²⁹ furthermore the former was done using the spherical approximation which would remove possible orientation dependence.

For small nanowires, one can compare a few of the *ab initio* calculations. Schmidt et al.¹⁷³ have found that the scaling rule $\Delta E_g \propto d^{-2}$ is valid for wires of size 2.13 nm and 1.80 nm, whereas it fails for a smaller wire (1.32 nm). The failure is attributed to the contribution of the surface. However, Li and Wang¹⁷⁶ have found the component $n_g = 1.23$ for wire size ranging from 2 to 4.3 nm. The band-gap changes of Ref. [173] are directly calculated within LDA, while the results of Ref. [176] have been corrected for the LDA error on the conduction-band effective mass. The justification for correcting the mass instead of the band gap is that the shape of the band structure is more important for getting the correct energy shift. However, this practice is sound only if the dispersion is parabolic and the wire is relatively large. Karanth and Fu,¹⁷⁸ using screened empirical

pseudopotential, have shown that the conduction band and valence band have rather different scaling components, $n_g \sim 1.2$ for the CBM and $n_g \sim 2.7$ for the VBM, with only small variations for different wire orientations. Pristine InP nanowires have been studied by Akiyama et al.,¹⁷⁴ mainly with the wurtzite structure. For very small wires, the CBM and VBM are found to derive from the surface dangling bonds, whereas for relatively large wires ($d > 1.35$ nm), the surface states become resonant and, thus, the CBM and

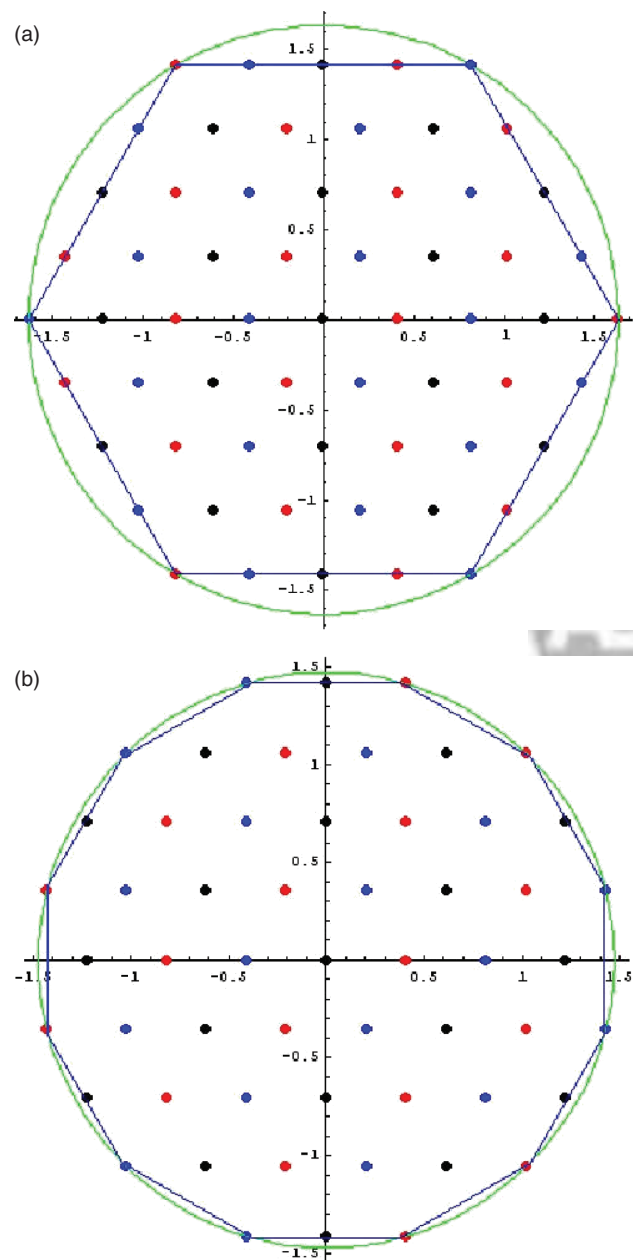


Fig. 13. Atomic positions of zincblende [111] nanowires projected onto the plane perpendicular to the wire axis. Black, red, and blue indicate atoms on three layers stacked along the wire axis. The horizontal axis is in the [11 $\bar{2}$] direction, and the vertical axis is in the [110] direction. (a) A “hexagonal” wire with radius = $2\sqrt{2}/3a$, containing 122 atoms/period. (b) A “dodecagonal” wire with radius = $\sqrt{13}/6a$, containing 110 atoms/period.

VBM are more bulk like. We would like to note that discussion of the scaling rule for nanowires with atomistic structures is somewhat ambiguous, because the nanowire shape, defined by the projection of the atoms onto the plane perpendicular to the wire axis, and thus the ratio of the area of a real nanowire to that of an ideal cylindrical wire depend on the chosen “wire diameter.” The wire shape may appear more faceted for certain diameters but more circular for others. For instance, the shape of a zincblende [111] nanowire could have a hexagonal shape^{173, 174} that have 6 atoms or a dodecagonal shape that have 12 atoms on the “wire surface,” as shown in Figure 13. Their areas are 83% and 95%, respectively, of a cylindrical wire.

Experimentally, there are few demonstrations of quantum confinement.^{52, 202} Gudiksen et al.⁵² observed signatures of quantum confinement for InP nanowires with diameters below 20 nm while Bhattacharya et al.⁵⁷ did not anticipate it at 50 nm. Both are consistent with our band-structure calculations.¹²⁹

Figure 14 presents recent calculations of the size dependence of the conduction-band mass. Since the two calculations were for nonoverlapping domains, comparison is difficult. The general trend is one of increasing mass with decreasing diameter for the lowest conduction state and the opposite behavior for valence states.¹⁷⁸ However, the two calculations do not quite match near 5 nm. While part of the difference could be attributed to different bulk masses used, it appears there are substantial differences in the two calculations. This shows the difficulty in computing accurate effective masses.

4.2.3. Wurtzite Nanowires

In addition to the one study of wurtzite InP NW's mentioned earlier in this section, there have been limited studies

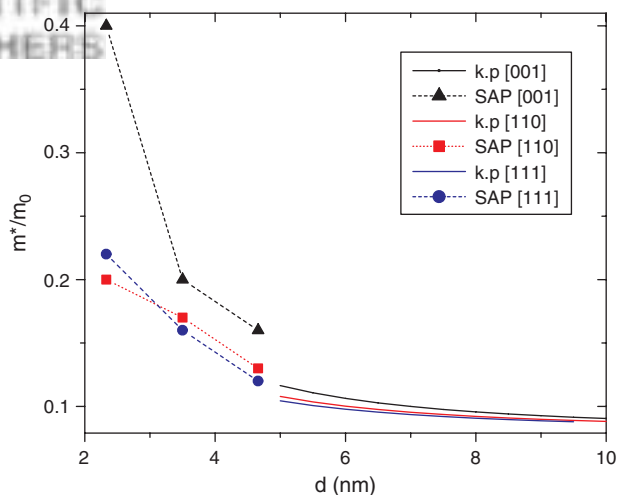


Fig. 14. Conduction-band effective mass for cylindrical [001], [110] and [111] InP nanowires. Reprinted with permission from [129], B. Lassen et al., *J. Mat. Res.* 21, 2927 (2006). © 2006, Materials Research Society; from [178], D. Karanth and H. Fu, *Phys. Rev. B* 74, 155312 (2006). © 2006, American Physical Society.

for AlN,^{33, 176, 214} CdS,¹⁷⁶ CdSe,^{38, 176} GaN,^{45, 48, 176} InN,¹⁷⁶ ZnO,^{176, 177} and ZnS.^{68, 176} An *ab initio* calculation of the size variation of the band gap for these semiconductors is shown in Figures 6 and 7. For CdSe, the available experimental and theoretical data are in very good agreement.

The electronic structures of wurtzite AlN nanowires have been calculated by Li and Wang with H-passivation,¹⁷⁶ and by Zhao et al.²¹⁴ with and without H-passivation. For the pristine structure, Zhao et al. have indicated that the VBM is derived from the N dangling bonds and the corresponding band shows very little dispersion, but the CBM is more bulk like and the band shows significant dispersion.

Xiang et al.¹⁷⁷ have calculated the electronic structure of wurtzite ZnO nanowires. They have found that the VBM is primarily derived from the surface O *2p*-like dangling bonds, whereas the CBM is more bulk like and the band is dispersive.

As mentioned in Section 4.2, in a couple of papers,^{33, 45} the wire diameter was extracted from Eq. (6) given the experimental band-gap shift. Thus, if the NW effective masses are different from the bulk values, then there would be a corresponding error in the size determination.

Orientational effect on the band structure had been measured for GaN⁴⁸ and calculated for ZnS.⁶⁸ For GaN, the measured gap difference for a 15 nm NW along the [001] and [10 $\bar{1}$ 0] is about 0.19 eV. The origin of the difference has yet to be ascertained and is unlikely to be purely from band-structure anisotropy. An unpublished calculation has shown the latter to be of the order of 20 meV if spontaneous polarization is not included in the calculation.²¹⁵ More recent work proposes surface trap states as responsible for explaining the difference.²¹⁶ For ZnS, the gap difference is around 10 meV at 5 nm.

4.3. Modulated Nanowires

We consider separately the electronic properties of modulated nanowires. Two types will be briefly discussed: axial and radial (or core/shell).

4.3.1. Axial

We recently predicted, on the basis of a parabolic one-band model with an infinite potential barrier outside the nanowire that a drastic change in the localization of electron states can occur below a certain critical radius for a NWSL.²¹⁷ That model was chosen because it leads to analytic solutions. The correctness of the physics was recently confirmed using a numerical approach.^{135, 218} Since then, a couple of TB calculations have also been carried out.^{155, 219} The calculation of Persson and Xu²¹⁹ confirmed our result though they reported smaller critical radii than we obtained.

4.3.2. Radial

An early form of a radially-modulated nanowire was the theoretical Russian Doll structure of Kim et al.²²⁰ in which

GaAs and AlAs cylindrical layers are nested within each other. They were able to obtain the puzzling result that electrons and holes can be spatially separated on different layers of the same material (GaAs) and still be derived from the same wave vector (Γ valleys). This remains to be confirmed experimentally.

More recent work has focussed on a core-shell structure.^{221, 222} They carried out an LDA-DFT calculation for Si-Ge NW's oriented along [111] and [110] as a function of composition $x = N_{\text{core}}/(N_{\text{core}} + N_{\text{shell}})$ and total atom number $N = N_{\text{core}} + N_{\text{shell}}$ for N up to ~ 150 per unit cell; the atomic structures are fully relaxed. The smallest size corresponds roughly to 1 nm diameter. The basic conclusion is that the (direct) band gap is blue shifted by an amount that depends upon N as follows:

$$E_g(N) = E_g(\infty) + \frac{A}{N} \quad (12)$$

and, thus, as $1/d^2$. Since the band-gap difference falls mostly on the valence band, the results could be understood largely in terms of quantum confinement of the hole. They also found that $\Delta E_g[111] > \Delta E_g[110]$.

In contrast to the Si/Ge system that has relatively small type-II energy alignment, core-shell nanowires based on GaN/GaP or ZnO/ZnSe with large type-II energy alignments have recently been investigated.¹⁸¹ The central finding is that the electron state at the CBM and the hole state at the VBM are, respectively, confined in the core and shell, resulting in an efficient charge separation. Additionally, the band gap is found to be tunable in a much larger range than that defined by the two components.

4.4. Quantum Rods

It is relevant to document briefly the electronic properties of QR's. Two aspects of the electronic structure of QR's that have been discussed relate to the dependence on the aspect ratio and the nature of the top of the valence band. A fit to room-temperature PL data by Hu et al.²²³ gave the following expression for the gap in terms of the length L and width W for CdSe QR's:

$$E_g = 1.8563 - \frac{2.0835}{L^2} + \frac{4.5507}{W^2} - 0.0018 \left(\frac{L}{W}\right)^2 + 0.0001 \left(\frac{L}{W}\right)^3 + \frac{10.5824}{L^3} - \frac{0.3833}{W^3} \quad (13)$$

Katz et al.²²⁴ did experiments on CdSe QR's; typical dimensions were 31 nm \times 1.9 nm and 11 nm \times 2.9 nm. They only carried out unpolarized PL and concentrated on the energy spectrum. The basic conclusion was that the energies were mostly sensitive to the radial confinement, down to an aspect ratio of about 2, and not on the length. The latter result is in rough agreement with $k \cdot p$ calculations by Lassen et al.¹³³ on InP QR's. Yorikawa et al.¹⁴⁶

had earlier done TB calculations for Si QR's and found the critical aspect ratios to be about 3.5, 5.5, and 8.5 for [001], [111], and [110] rods, respectively. While they had commented that those are surprisingly small, we see that they are in fact bigger than the ones for CdSe QR's. Indeed, scanning tunneling spectroscopy and PL experiments on InAs QR's²²⁵ showed a distinct length dependence of the band gap up to an aspect ratio of at least 4. The difference in behaviour between CdSe and InAs QR's has been attributed to the ratio of the Bohr radius to the QR length.²²⁵

Regarding the nature of the valence states, Hu et al.³⁷ did empirical pseudopotential calculations which gave a level crossing at an aspect ratio of 1.5–2 and is consistent with their observation of polarization cross-over for CdSe. The model used is a spherical dot with 1.5 nm with an added cylindrical segment along the *c*-axis. Our band-structure calculations for a cylindrical zincblende InGaAs QR also revealed the possibility of a level crossing,¹³³ but this was not found by Li and Xia in their six-band calculation for a spheroidal CdSe QR.²²⁶ Katz et al.²²⁴ also studied CdSe QR's. The theoretical model used is an infinite barrier along the *z*-direction, and a cylindrical QWR with a 5 eV barrier for parabolic electrons and an infinite barrier for four-band holes within the axial approximation; they did not report any level crossing either. Finally, to complicate matters, Li and Wang²²⁷ clearly state that there is no level crossing in zincblende QR's since the crossing arises from the crystal-field splitting in the bulk valence-band structure of wurtzite crystals. There is, thus, no apparent consistency among the above results.

5. POLARIZED OPTICAL PROPERTIES

We end the review of properties by including a discussion of the optical properties of nanowires and quantum rods

since the latter problem has received substantial interest recently and the theory is closely related to nanowire band-structure calculations.

5.1. Nanowires

To set the stage for this discussion, we start by summarizing the main conclusion of Wang et al.¹⁰⁴ Both excitation and emission spectroscopy on single InP nanowires displayed substantial (>90%) polarization anisotropy that is more or less independent of the wire widths (10–50 nm), over most of the PL peak, for different excitation wavelengths (488 nm and 514 nm), and significantly higher than previously reported anisotropies for embedded quantum wires (over 10 times larger in the ratio of PL intensities). A summary of reported results are given in Table VI.

Similar results had earlier been obtained for QWR's.^{113, 114, 191, 228} Calculations, all of which were obtained using a four-band *k*·*p* model, for cylindrical QWR's result in polarized absorption along the axis to be four times stronger than in-plane, which Sercel and Vahala¹⁹¹ attributed to be in agreement with experimental data.^{113, 114} Similar results to Sercel and Vahala were obtained by Vurgaftman et al. in 1994²²⁸ for a 10 nm × 10 nm square QWR GaAs/Al_{0.3}Ga_{0.7}As. Overall, the earlier calculation of quantum-confinement origin leads to a polarization ratio $\rho \leq 0.6$ (see Eq. (14)).

For cubic (diamond and zincblende) NW's, all experiments agree on the basic observation that the light emission is polarized along the wire axis. A measure of the polarization can be defined as follows:

$$\rho = \frac{I_{\parallel} - I_{\perp}}{I_{\parallel} + I_{\perp}} \quad (14)$$

where I_{\parallel} (I_{\perp}) refers to the intensity along (perpendicular) to the wire axis. Clues to the explanation of the

Table VI. Polarized response of quantum wires and nanowires.

	Diameter (nm)	Wavelength (nm)	Expt	ρ	
				Dielectric theory	Band-structure theory
AlGaAs V-groove	2.5 ¹¹⁶	488, 710	0.6, 0.3		
AlGaAs T-QWR	5 ¹¹⁵	~800	0.39 (PLE), 0.2 (PL)		0.34
AlGaAs QWR	10 ¹⁹¹				0.6
Si	~4 ¹¹⁷ ~20 ¹¹⁸	500 >500	0.5 0.94	0.62 0.95	
InP	10–50 ¹⁰⁴ 5.8 ¹⁴⁸ 6–20 ¹³⁰	488, 514	0.91 ± 0.07	0.96	1 0.9–0.6
GaN	15 ²⁰	254	0.16		
CdSe	~20 ¹¹⁹ ~20 ⁴⁰	690 690	~0.4 ~0.5		
ZnO ⁶⁵	30–150	365–600	0.13–0.18		

polarization are as follows. In the case of PL experiments, the polarization is independent of the polarization of the excitation;¹¹⁷ in the latter work, the luminescence was also postulated to emanate from an oxygen defect at the nanowire surface (emission energy of about 2.45 eV which is clearly much higher than the bulk indirect gap). In Ref. [65], the polarization is in the photoconductivity. Polarization larger than allowed by the early $k \cdot p$ theory led to the proposal of dielectric mismatch as the origin of the polarization.^{104, 117, 118, 229}

From a recent *ab initio* calculation Karanth and Fu¹⁷⁸ have found that the interband optical transition of the InP nanowire is generally polarized along the direction of the wire axis. However, the polarization decreases with decreasing wire size, which is interpreted in terms of the observation that the magnitude of the matrix element is found to be primarily determined by that of the bulk at $k_0 \sim 1/d$. It is in fact not so straightforward to understand the sign of the polarization. It has been well known that for a quantum well or superlattice with the presence of only simple quantum confinement (e.g., GaAs/AlGaAs system that does not have the complication caused by strain), the optical transition is polarized in the plane perpendicular to the direction of the modulation. It has also been found that with the presence of a two-dimensional modulation, the optical transition is then polarized along the remaining direction that is not subjected to the modulation.²³⁰ If the quantum confinement is assumed to be in the x - y plane, and given that the valence band-edge states in a bulk zincblende material are $|X\rangle$, $|Y\rangle$, and $|Z\rangle$ -like (neglecting spin-orbit interaction), and the conduction band edge is $|S\rangle$ -like, from the point of view of perturbation, the band-edge state of the quantum confined structure will be $|Z\rangle$ -like, thus, the optical transition is expected to be polarized along the z direction (here the wire axis). However, the band derived from the $|Z\rangle$ -like state has a smaller mass than that derived from the $|X\rangle$ and $|Y\rangle$ -like states in the bulk, and based on this consideration one expects that the band-edge state in the wire is derived from the band of heavier mass. Thus, the polarization in the nanowire will be determined by the interplay of the two effects: the quantum confinement and the $k \cdot p$ coupling of the HH and LH in the bulk. For the case of strong confinement typically encountered in a free-standing nanowire, the polarization is likely to be along the wire axis, because of the large “crystal-field splitting” between the $|Z\rangle$ and $|X\rangle$ or $|Y\rangle$ -like states. With the spin-orbit interaction included, the analysis remains qualitatively the same, but $|3/2, 3/2\rangle$ takes the position of $|X\rangle$ or $|Y\rangle$ and $|3/2, 1/2\rangle$ the position of $|Z\rangle$.

However, the $k \cdot p$ calculations of Maslov and Ning¹³⁰ indicate that the polarization anisotropy of an InP nanowire should decrease from 90% to 60% as the diameter increases from 6 to 20 nm; they were able to obtain a diameter dependence by going beyond the four-band

model used by Sercel and Vahala for QWR's. Karanth and Fu¹⁷⁸ and Persson and Xu¹⁴⁸ claim that band-structure effects alone could lead to polarization near 100% and since they studied nanowires smaller than 5 nm, their conclusions do not contradict Maslov and Ning. However, the $k \cdot p$ result that the anisotropy is around 60% near 10 nm does not agree with the experimental value of near 100% obtained by Wang et al.¹⁰⁴ We note the following regarding InP NW's. As pointed out by Wang et al.¹⁰⁴ and as Figure 12 clearly show, quantum confinement is not important until one reaches a diameter smaller than roughly 20 nm. Thus, the absence of size dependence in the experimental data is not proof that the mechanism is not due to quantum confinement. What appears to have been shown by the above work is that the latter alone cannot explain the polarization in nanowires with diameters greater than 10 nm. Indeed, it is quite likely that the large anisotropy for thick NW's is due mainly to dielectric effects and that for thin NW's would be due to quantum confinement.

For wurtzite NW's, the few experiments actually yield two different answers.^{40, 119} The discrepancy appears to have been resolved in a recent paper⁴⁰ where they correlate the interplay of the dielectric mismatch and band structure to the relative size of the nanostructure and the wavelength of the electromagnetic field. Specifically, the argument proposed is that the dielectric mismatch only plays a role if the wavelength of light is long compared to the dimension and they showed that band-structure effects did not play a role in their 70 nm NW's by growing them along and perpendicular to the c axis and getting the same response. However, their statement of “strong polarization dependence” does not match the value of 50% that we extracted from their Figure 3(b); their other figures give even smaller polarization ratios. Maslov and Ning¹³⁶ again found that quantum confinement alone leads to a polarization anisotropy of an GaN nanowire that should decrease as the radius increases and the polarization is predominantly along the axis for a radius near 3.5 nm.

5.2. Quantum Rods

A number of experiments have demonstrated the strong linear polarization of optical emission from QR's.^{37, 180, 231} Hu et al.^{37, 223} did empirical pseudopotential calculations which gave a transition to z -polarized optical emission at an aspect ratio of 1.5–2 and is consistent with their experiments. The theory indicates it is due to a level crossing in the valence band. They discount the dielectric model (concentration of field lines in high dielectric constant regions) as the mechanism for the linear polarization. Our band-structure calculations for a cylindrical InP QR also revealed the possibility of a level crossing,¹³³ even though this was not observed by Li and Xia²²⁶ in their six-band calculation for a spheroidal QR. A different mechanism, the fine structure of one-dimensional excitons, has also

been proposed as the origin of the linear polarization of PL.²³² Thus, we do not believe there is a definitive explanation of the extreme polarization yet.

For both the nanowire and QR cases, we have not included the data of Hsu et al.⁹⁷ on ZnO nanorods since the aspect ratio of the nanorods was not given. We will mention, nevertheless, their peculiar observation that the polarization of the UV (band-edge) emission (along the rod axis which is also the *c* axis) is 90° out-of-phase with respect to that of the green (defect) emission.

6. SUMMARY

The above is a brief overview of the main theories and experiments that probe the electronic properties of semiconductor nanowires. The main findings are as follows. Most of the calculations have been first-principles ones but they have been restricted to small sized nanowires (typically less than 10 nm). *k* · *p* calculations should probably only be used for diameters greater than ~2 nm, while tight-binding calculations can bridge the two domains and have been carried out for nanowires as large as 40 nm. The first-principles and tight-binding calculations require a model of passivation though no detailed studies have been carried out of the impact of different passivation for the latter method. Indeed, one general conclusion is that the passivation model plays an important role on the electronic properties for small nanowires. The different methods have often used slightly different shapes though this effect is expected to be less significant. The literature also shows a paucity of calculations beyond the single-particle picture (i.e., incorporation of dielectric mismatch and Coulomb interaction effects) necessary for a proper comparison to optical data such as photoluminescence. All the methods show that the single-particle band gap rarely scales as the inverse square of the size. There are too few data on effective masses for a consistent quantitative comparison of the various methods, though there is agreement on the trend of increasing conduction-band effective mass with decreasing diameter for InP nanowires. Finally, we believe the origin of the polarization anisotropy for both nanowires and quantum rods is still somewhat unclear. Overall, the level of accuracy of the theories is expected to be of the order of 100–200 meV at best. Experimentally, while band gaps can be determined fairly accurately, size determination remains less so. There is a need for additional studies on very small nanowires.

Acknowledgments: This work was supported by a Balslev award (Denmark), an NSF CAREER award (NSF Grant Nos. 9984059, 0454849), and by a Research Challenge grant from Wright State University and the Ohio Board of Regents. Work at NREL was supported by a NREL LDRD program (# 06590504). We would like to thank Dr. Jingbo Li for providing some of the data used in this review.

References and Notes

1. K. V. Klitzing, G. Dorda, and M. Pepper, *Phys. Rev. Lett.* **45**, 494 (1980).
2. D. C. Tsui and A. C. Gossard, *Appl. Phys. Lett.* **38**, 550 (1981).
3. B. J. van Wees, H. van Houten, C. W. J. Beenakker, J. G. Williamson, L. P. Kouwenhoven, D. van der Marel, and C. T. Foxon, *Phys. Rev. Lett.* **60**, 848 (1988).
4. I. Giaever and H. R. Zeller, *Phys. Rev. Lett.* **20**, 1504 (1968).
5. B. Su, V. J. Goldman, and J. E. Cunningham, *Science* **255**, 313 (1992).
6. H. Sakaki, *Jap. J. Appl. Phys.* **19**, L735 (1980).
7. Y. Zhang, M. D. Sturge, K. Kash, B. P. V. der Gaag, A. S. Gozdz, L. T. Florez, and J. P. Harbison, *Phys. Rev. B* **51**, 13303 (1995).
8. Z. I. Alferov, *Rev. Mod. Phys.* **73**, 767 (2001).
9. M. Law, L. Greene, J. Johnson, R. Saykally, and P. Yang, *Nat. Mater.* **4**, 455 (2005).
10. H. Pettersson, J. Trägårdh, A. I. Persson, L. Lin, D. Hessman, and L. Samuelson, *Nano Lett.* **6**, 229 (2006).
11. Y. Cui, X. Duan, Y. Huang, and C. M. Lieber, *Nanowires and Nanobelts*, edited by Z. L. Wang, Kluwer, Boston (2003), Vol. I, Chap. 1, pp. 1–68.
12. K. Hiruma, M. Yazawa, T. Katsuyama, K. Ogawa, K. Haraguchi, M. Koguchi, and H. Kakibayashi, *J. Appl. Phys.* **77**, 2 (1995).
13. X. Duan and C. M. Lieber, *Adv. Mater.* **12**, 298 (2000).
14. P. Yang, Y. Wu, and R. Fan, *Int. J. Nanoscience* **1**, 1 (2002).
15. M. Law, J. Goldberger, and P. Yang, *Annual Review of Materials Research* **34**, 83 (2004).
16. Z. L. Wang, *Nanowires and Nanobelts*, Kluwer, Boston (2003).
17. D. R. Bowler, *J. Phys. Condens. Matter* **16**, R721 (2004).
18. *Materials Today* **9**(October) (2006).
19. P. M. Petroff, A. C. Gossard, R. A. Logan, and W. Wiegmann, *Appl. Phys. Lett.* **41**, 635 (1982).
20. W. Wegscheider, L. Pfeiffer, M. Dignam, A. Pinzucuk, K. West, and R. Hull, *Semicond. Sci. Technol.* **9**, 1933 (1994).
21. K. Kash, B. P. V. der Gaag, D. D. Mahoney, A. S. Gozdz, L. T. Florez, J. P. Harbison, and M. D. Sturge, *Phys. Rev. Lett.* **67**, 1326 (1991).
22. A. Gustafsson, F. Reinhardt, G. Biasiol, and E. Kapon, *Appl. Phys. Lett.* **67**, 3673 (1995).
23. A. M. Morales and C. M. Lieber, *Science* **279**, 208 (1998).
24. Z. W. Pan, Z. R. Dai, and Z. L. Wang, *Science* **291**, 1947 (2001).
25. F. G. Tarntair, C. Y. Wen, L. C. Chen, J.-J. Wu, K. H. Chen, P. F. Kuo, S. W. Chang, Y. F. Chen, W. K. Hong, and H. C. Cheng, *Appl. Phys. Lett.* **76**, 2630 (2000).
26. L. J. Lauhon, M. S. Gudiksen, D. Wang, and C. M. Lieber, *Nature* **420**, 57 (2002).
27. M. S. Gudiksen, L. J. Lauhon, J. Wang, D. C. Smith, and C. M. Lieber, *Nature* **415**, 617 (2002).
28. Y. Wu, R. Fan, and P. Yang, *Nano Lett.* **2**, 83 (2002).
29. M. T. Björk, B. J. Ohlsson, T. Sass, A. I. Persson, C. Thelander, M. H. Magnusson, K. Deppert, L. R. Wallenberg, and L. Samuelson, *Nano Lett.* **2**, 87 (2002).
30. S. Iijima, *Nature* **354**, 56 (1991).
31. M. Kappelt, M. Grundmann, A. Krost, V. Türck, and D. Bimberg, *Appl. Phys. Lett.* **68**, 3596 (1996).
32. Q. L. Liu, T. Tanaka, J. Q. Hu, F. F. Xu, and T. Sekiguchi, *Appl. Phys. Lett.* **83**, 4939 (2003).
33. Q. Zhao, H. Zhang, X. Xu, Z. Wang, J. Xu, D. Yu, G. Li, and F. Su, *Appl. Phys. Lett.* **86**, 193101 (2005).
34. X. Duan, Y. Huang, R. Agarwal, and C. M. Lieber, *Nature* **421**, 241 (2003).
35. T. B. Hoang, L. V. Titova, H. E. Jackson, L. M. Smith, J. M. Yarrison-Rice, J. L. Lensch, and L. J. Lauhon, *Appl. Phys. Lett.* **89**, 123123 (2006).

36. L. V. Titova, T. B. Hoang, H. E. Jackson, L. M. Smith, J. M. Yarrison-Rice, Y. Kim, H. J. Joyce, H. H. Tan, and C. Jagadish, *Appl. Phys. Lett.* 89, 73126 (2006).
37. J. Hu, L.-S. Li, W. Yang, L. Manna, L.-W. Wang, and A. P. Alivisatos, *Science* 292, 2060 (2001).
38. H. Yu, J. Li, R. A. Loomis, P. C. Gibbons, L.-W. Wang, and W. E. Buhro, *J. Am. Chem. Soc.* 125, 16168 (2003).
39. S. J. Kwon, Y.-J. Choi, J.-H. Park, I.-S. Hwang, and J.-G. Park, *Phys. Rev. B* 72, 205312 (2005).
40. C. X. Shan, Z. Liu, and S. K. Hark, *Phys. Rev. B* 74, 153402 (2006).
41. Z. H. Wu, X. Mei, D. Kim, M. Blumin, H. E. Ruda, J. Q. Liu, and K. L. Kavanagh, *Appl. Phys. Lett.* 83, 3368 (2003).
42. Z. H. Wu, M. Sun, X. Y. Mei, and H. E. Ruda, *Appl. Phys. Lett.* 85, 657 (2004).
43. K. Tatenno, H. Gotoh, and Y. Watanabe, *Appl. Phys. Lett.* 85, 1808 (2004).
44. W. Han, S. Fan, Q. Li, and Y. Hu, *Science* 277, 1287 (1997).
45. M. W. Lee, H. Z. Twu, C.-C. Chen, and C.-H. Chen, *Appl. Phys. Lett.* 79, 3693 (2001).
46. Z. Zhong, F. Qian, D. Wang, and C. M. Lieber, *Nano Lett.* 3, 343 (2003).
47. T. Kuykendall, P. Pauzauskie, S. Lee, Y. Zhang, J. Goldberger, and P. Yang, *Nano Lett.* 3, 1063 (2003).
48. T. Kuykendall, P. Pauzauskie, Y. Zhang, J. Goldberger, D. Sibuly, J. Denlinger, and P. Yang, *Nat. Mater.* 3, 524 (2004).
49. J. Zhang, L. Zhang, X. Peng, and X. Wang, *J. Mater. Chem.* 12, 802 (2002).
50. M. He, M. M. E. Fahmi, S. N. Mohammad, R. N. Jacobs, L. Salamanca-Riba, F. Felt, M. Jah, A. Sharma, and D. Lakin, *Appl. Phys. Lett.* 87, 3749 (2003).
51. H. D. Park, S. M. Prokes, and R. C. Cammarata, *Appl. Phys. Lett.* 87, 063110 (2005).
52. M. S. Gudiksen, J. Wang, and C. M. Lieber, *J. Phys. Chem. B* 106, 4036 (2002).
53. H. Yu, J. Li, R. A. Loomis, L.-W. Wang, and W. E. Buhro, *Nat. Mater.* 2, 517 (2003).
54. P. J. Poole, J. Lefebvre, and J. Fraser, *Appl. Phys. Lett.* 83, 2055 (2003).
55. Ü. Krishnamachari, M. Borgstrom, B. J. Ohlsson, N. Panev, L. Samuelson, W. Seifert, M. W. Larsson, and L. R. Wallenberg, *Appl. Phys. Lett.* 85, 2077 (2004).
56. D. S. Kim, J. Y. Lee, C. W. Na, S. W. Yoon, S. Y. Kim, J. Park, Y. Jo, and M.-H. Jung, *J. Phys. Chem. B* 110, 18262 (2006).
57. S. Bhattacharya, D. Banerjee, K. W. Adu, S. Samui, and S. Bhattacharyya, *Appl. Phys. Lett.* 85, 2008 (2004).
58. D. D. D. Ma, C. S. Lee, F. C. K. Au, S. Y. Tong, and S. T. Lee, *Science* 299, 1874 (2003).
59. H.-K. Seong, H.-J. Choi, S.-K. Lee, J.-I. Lee, and D.-J. Choi, *Appl. Phys. Lett.* 85, 1256 (2004).
60. Y. C. Kong, D. P. Yu, B. Zhang, W. Fang, and S. Q. Feng, *Appl. Phys. Lett.* 78, 407 (2001).
61. M. H. Huang, S. Mao, H. Feick, H. Yan, Y. Wu, H. Kind, E. Weber, R. Russo, and P. Yang, *Science* 292, 1897 (2001).
62. D. Banerjee, J. Y. Lao, D. Z. Wang, J. Y. Huang, Z. F. Ren, D. Steeves, B. Kimball, and M. Sennett, *Appl. Phys. Lett.* 83, 2061 (2003).
63. Y. W. Heo, L. C. Tien, D. P. Norton, B. S. Kang, F. Ren, B. P. Gila, and S. J. Pearton, *Appl. Phys. Lett.* 85, 2002 (2004).
64. Y. W. Heo, L. C. Tien, Y. Kwon, D. P. Norton, S. J. Pearton, B. S. Kang, and F. Ren, *Appl. Phys. Lett.* 85, 2274 (2004).
65. Z. Fan, P. C. Chang, J. G. Lu, E. C. Walter, R. M. Penner, C. H. Lin, and H. P. Lee, *Appl. Phys. Lett.* 85, 6128 (2004).
66. Y. Wang, L. Zhang, C. Liang, G. Wang, and X. Peng, *Chem. Phys. Lett.* 317, 314 (2002).
67. J. X. Ding, J. A. Zapien, W. W. Chen, Y. Lifshitz, S. T. Lee, and X. M. Meng, *Appl. Phys. Lett.* 85, 2361 (2004).
68. Q. Xiong, G. Chen, J. D. Accord, X. Liu, J. J. Zengel, H. Gutierrez, J. M. Redwing, L. C. Lew Yan Voon, B. Lassen, and P. C. Eklund, *Nano Lett.* 4, 1663 (2004).
69. Y. F. Chan, X. F. Duan, S. K. Chan, I. K. Sou, X. X. Zhang, and N. Wang, *Appl. Phys. Lett.* 83, 2665 (2003).
70. C. X. Shan, Z. Liu, X. T. Zhang, C. C. Wong, and S. K. Hark, *Nanotechnology* 17, 5561 (2006).
71. X. Y. Huang, J. Li, Y. Zhang, and A. Mascarenhas, *J. Am. Chem. Soc.* 125, 7049 (2003).
72. H. Yu, J. Li, R. A. Loomis, L.-W. Wang, and W. E. Buhro, *Nat. Mater.* 2, 517 (2003).
73. X. T. Zhang, Z. Liu, K. M. Ip, Y. P. Leung, Q. Li, and S. K. Hark, *J. Appl. Phys.* 95, 5752 (2004).
74. R. Wagner and W. Ellis, *Appl. Phys. Lett.* 4, 89 (1964).
75. Y. Wu and P. Yang, *J. Am. Chem. Soc.* 123, 3165 (2001).
76. A. I. Persson, M. W. Larsson, S. Stenström, B. J. Ohlsson, L. Samuelson, and L. R. Wallenberg, *Nat. Mater.* 3, 677 (2004).
77. K. A. Dick, K. Deppert, T. Martensson, M. Bernhard, L. Samuelson, and W. Seifert, *Nano Lett.* 5, 761 (2005).
78. T. J. Trentler, K. M. Hickman, S. C. Goel, A. M. Viano, P. C. Gibbons, and W. E. Buhro, *Science* 270, 1791 (1995).
79. G. Zou, H. Li, Y. Zhang, K. Xiong, and Y. Qian, *Nanotechnology* 11, S313 (2006).
80. P. S. Shah, T. Hanrath, K. P. Johnston, and B. A. Korgel, *J. Phys. Chem. B* 108, 9574 (2004).
81. A. O'Neil and J. Watkins, *MRS Bull.* 30, 967 (2005).
82. E. Givargizov, *J. Cryst. Growth* 31, 20 (1975).
83. Q. Xiong, R. Gupta, K. W. Adu, E. C. Dickey, G. D. Lian, D. T. J. E. Fischer, and P. C. Eklund, *J. Nanosci. Nanotechnol.* 3, 335 (2003).
84. Y. Cui, X. Duan, J. Hu, and C. M. Lieber, *J. Phys. Chem. B* 104, 5213 (2005).
85. X. Chen, J. Xu, R. Wang, and D. Yu, *Advan. Mater.* 15, 419 (2003).
86. S. Gradec-Caronak, F. Qian, Y. Li, H.-G. Park, and C. M. Lieber, *Appl. Phys. Lett.* 87, 173111 (2005).
87. Y. Wu and P. Yang, *Chem. Mater.* 12, 605 (2000).
88. P. Yang, H. Yan, S. Mao, R. Russo, J. Johnson, R. Saykally, N. Morris, J. Pham, R. He, and H.-J. Choi, *Adv. Funct. Mater.* 12, 323 (2002).
89. Z. Wang, *J. Phys. Condens. Matter* 16, R829 (2004).
90. Z. Wang, *Annu. Rev. Phys. Chem.* 55, 159 (2004).
91. L.-S. Li, J. Hu, W. Yang, and A. P. Alivisatos, *Nano Lett.* 1, 349 (2001).
92. X. Zhang, Z. Liu, C. Wong, and S. Hark, *Solid State Commun.* 139, 387 (2006).
93. S. P. Ahrenkiel, O. I. Mii, A. Miedaner, C. J. Curtis, J. M. Nedeljkovi, and A. J. Nozik, *Nano Lett.* 3, 833 (2003).
94. S. Kan, T. Mokari, E. Rothenberg, and U. Banin, *Nat. Mater.* 2, 155 (2003).
95. E. Lifshitz, M. Bashouti, V. Kloper, A. Kigel, M. S. Eisen, and S. Berger, *Nano Lett.* 3, 857 (2003).
96. Y. Gu, I. L. Kuskovsky, M. Yin, S. O'Brien, and G. F. Neumark, *Appl. Phys. Lett.* 85, 3833 (2004).
97. N. E. Hsu, W. K. Hung, and Y. F. Chen, *J. Appl. Phys.* 96, 4671 (2004).
98. Y. Cao and U. Banin, *J. Am. Chem. Soc.* 122, 9692 (2000).
99. F. Qian, Y. Li, S. Gradecak, D. Wang, C. J. Barrelet, and C. M. Lieber, *Nano Lett.* 4, 1975 (2004).
100. Y.-J. Hsu, S.-Y. Lu, and Y.-F. Lin, *Adv. Funct. Mater.* 15, 1350 (2005).
101. J. Noborisaka, J. Motohisa, S. Hara, and T. Fukui, *Appl. Phys. Lett.* 87, 093109 (2005).
102. R. Solanki, J. Huo, J. L. Freeouf, and B. Miner, *Appl. Phys. Lett.* 81, 3864 (2002).
103. M. W. Larsson, J. B. Wagner, M. Wallin, P. Hakansson, L. E. Fröberg, L. Samuelson, and L. R. Wallenberg, *Nanotechnology* 18, 015504 (2007).

104. J. Wang, M. S. Gudiksen, X. Duan, Y. Cui, and C. M. Lieber, *Science* 293, 1455 (2001).
105. M. T. Björk, B. J. Ohlsson, T. Sass, A. I. Persson, C. Thelander, M. H. Magnusson, K. Deppert, L. R. Wallenberg, and L. Samuelson, *Appl. Phys. Lett.* 80, 1058 (2002).
106. Y. J. Xing, Z. H. Xi, Z. Q. Xue, X. D. Zhang, J. H. Song, R. M. Wang, J. Xu, Y. Song, S. L. Zhang, and D. P. Yu, *Appl. Phys. Lett.* 83, 1689 (2003).
107. J. Goldberger, R. He, Y. Zhang, S. Lee, H. Yan, H.-J. Choi, and P. Yang, *Nature* 422, 599 (2003).
108. Q. Xiong, J. Wang, P. C. Eklund, O. Reese, and L. C. Lew Yan Voon, *Nano Lett.* 4, 1991 (2004).
109. D. D. D. Ma, C. S. Lee, F. C. K. Au, S. Y. Tong, and S. T. Lee, *Science* 299, 1874 (2003).
110. M. Mattila, T. Hakkarainen, M. Mulot, and H. Lipsanen, *Nanotechnology* 17, 1580 (2006).
111. H. J. Fan, R. Scholz, M. Zacharias, U. Gösele, F. Bertram, D. Forster, and J. Christen, *Appl. Phys. Lett.* 86, 023113 (2005).
112. L. V. Titova, T. B. Hoang, H. E. Jackson, L. M. Smith, J. M. Yarrison-Rice, Y. Kim, H. J. Joyce, H. H. Tan, and C. Jagadish, *Appl. Phys. Lett.* 89, 053119 (2006).
113. M. Tsuchiya, J. M. Gaines, R. H. Yan, R. J. Simes, P. O. Holtz, L. A. Coldren, and P. M. Petroff, *Phys. Rev. Lett.* 62, 466 (1989).
114. M. Kohl, D. Heitmann, P. Grambow, and K. Ploog, *Phys. Rev. Lett.* 63, 2124 (1989).
115. H. Akiyama, T. Someya, and H. Sakaki, *Phys. Rev. B* 53, R4229 (1996).
116. F. Vouilloz, D. Y. Oberli, M.-A. Dupertuis, A. Gustafsson, F. Reinhardt, and E. Kapon, *Phys. Rev. B* 57, 12378 (1998).
117. J. Qi, A. M. Belcher, and J. M. White, *Appl. Phys. Lett.* 82, 2616 (2003).
118. D. D. D. Ma, S. T. Lee, and J. Shinar, *Appl. Phys. Lett.* 87 (2005).
119. R. Venugopal, P.-I. Lin, C.-C. Liu, and Y.-T. Chen, *J. Am. Chem. Soc.* 127, 11262 (2005).
120. S. Han, W. Jin, D. Zhang, T. Tang, C. Li, X. Liu, Z. Liu, B. Lei, and C. Zhou, *Chem. Phys. Lett.* 389, 176 (2004).
121. M. Saraydarov, V. Donchev, K. Germanova, X. L. Wang, S. J. Kim, and M. Ogura, *J. Appl. Phys.* 95, 64 (2004).
122. P. Yu, J. M. Nedeljkovic, P. A. Ahrenkiel, R. J. Ellingson, and A. J. Nozik, *Nano Lett.* 4, 1089 (2004).
123. Y. Huang, X. Duan, Y. Cui, and C. M. Lieber, *Nano Lett.* 2, 101 (2002).
124. M. G. Burt, *Semicond. Sci. Technol.* 3, 739 (1988).
125. G. Bastard, *Wave Mechanics Applied to Semiconductor Heterostructures*, Les Editions de Physique, Les Ulis (1988).
126. B. A. Foreman, *Phys. Rev. B* 54, 1909 (1996).
127. M. G. Burt, *J. Phys. Cond. Matter* 4, 6651 (1992).
128. P. Löwdin, *J. Chem. Phys.* 19, 1396 (1951).
129. B. Lassen, M. Willatzen, R. Melnik, and L. C. Lew Yan Voon, *J. Mater. Res.* 21, 2927 (2006).
130. A. V. Maslov and C. Z. Ning, *Phys. Rev. B* 72, 161310(R) (2005).
131. C. Galeriu, L. C. Lew Yan Voon, R. N. Melnik, and M. Willatzen, *Comp. Phys. Commun.* 157, 147 (2004).
132. W. Yang and K. Chang, *Phys. Rev. B* 72, 233309 (2005).
133. L. C. Lew Yan Voon, B. Lassen, R. Melnik, and M. Willatzen, *Nano Lett.* 4, 289 (2004).
134. B. Lassen, L. C. Lew Yan Voon, R. Melnik, and M. Willatzen, *Solid State Commun.* 132, 141 (2004).
135. L. C. Lew Yan Voon, B. Lassen, R. Melnik, and M. Willatzen, *J. Appl. Phys.* 96, 4660 (2004).
136. A. V. Maslov and C. Z. Ning, *Phys. Rev. B* 72, 125319 (2005).
137. E. I. Rashba, *Sov. Phys. Solid State* 1, 368 (1959).
138. G. E. Pikus, *Sov. Phys. JETP* 41, 1075 (1962).
139. Y. M. Sirenko, J. Jeon, K. W. Kim, and M. A. Littlejohn, *Phys. Rev. B* 53, 1997 (1996).
140. S. L. Chuang and C. S. Chang, *Phys. Rev. B* 54, 2491 (1996).
141. F. Mireles and S. E. Ulloa, *Phys. Rev. B* 60, 13659 (1999).
142. P. C. Sercel and K. J. Vahala, *Phys. Rev. B* 42, 3690 (1990).
143. L. C. Lew Yan Voon, C. Galeriu, B. Lassen, M. Willatzen, and R. Melnik, *Appl. Phys. Lett.* 87, 041906 (2005).
144. Y. Arakawa, T. Yamauchi, and J. N. Schulman, *Phys. Rev. B* 43, 4732 (1991).
145. G. D. Sanders and Y.-C. Chang, *Phys. Rev. B* 45, 9202 (1992).
146. H. Yorikawa, H. Uchida, and S. Muramatsu, *J. Appl. Phys.* 79, 3619 (1996).
147. M. P. Persson and H. Q. Xu, *Appl. Phys. Lett.* 81, 1309 (2002).
148. M. P. Persson and H. Q. Xu, *Phys. Rev. B* 70, 161310(R) (2004).
149. M. P. Persson and H. Q. Xu, *Nano Lett.* 4, 2409 (2004).
150. Y. Zheng, C. Rivas, R. Lake, K. Alam, T. Boykin, and G. Klimeck, *IEEE Trans. Electron Devices* 52, 1097 (2005).
151. X. Guan and Z. Yu, *IEEE Conference on Electron Devices and Solid-State Circuits*, IEEE (2005), pp. 19–22.
152. C. Harris and E. P. O'Reilly, *Physica E* 32, 341 (2006).
153. M. P. Persson and H. Q. Xu, *Phys. Rev. B* 73, 125346 (2006).
154. Y. M. Niquet, A. Lherbier, N. H. Quang, M. V. Fernández-Serra, X. Blase, and C. Delerue, *Phys. Rev. B* 73, 165319 (2006).
155. Y. M. Niquet, *Phys. Rev. B* 74, 155304 (2006).
156. M. Luisier, A. Schenk, W. Fichtner, and G. Klimeck, *Phys. Rev. B* 74, 205323 (2006).
157. P. Vogl, H. P. Hjalmarson, and J. D. Dow, *J. Phys. Chem. Solids* 44, 365 (1983).
158. L. C. Lew Yan Voon, Worcester Polytechnic Institute, Worcester, Massachusetts (1993).
159. A. J. Read, R. J. Needs, K. J. Nash, L. T. Canham, P. D. J. Calcott, and A. Qteish, *Phys. Rev. Lett.* 69, 1232 (1992).
160. A. J. Read, R. J. Needs, K. J. Nash, L. T. Canham, P. D. J. Calcott, and A. Qteish, *Phys. Rev. Lett.* 70, 2050 (1993).
161. F. Buda, J. Kohanoff, and M. Parrinello, *Phys. Rev. Lett.* 69, 1272 (1992).
162. T. Ohno, K. Shiraishi, and T. Ogawa, *Phys. Rev. Lett.* 69, 2400 (1992).
163. M. S. Hybertsen and M. Needels, *Phys. Rev. B* 48, 4608 (1993).
164. B. Delley and E. F. Steigmeier, *Appl. Phys. Lett.* 67, 2370 (1995).
165. A. M. Saitta, F. Buda, G. Fiumara, and P. V. Giaquinta, *Phys. Rev. B* 53, 1446 (1996).
166. X. Zhao, C. M. Wei, L. Yang, and M. Y. Chou, *Phys. Rev. Lett.* 92, 236805 (2004).
167. T. Yo, A. J. Williamson, and G. Galli, *Phys. Rev. B* 74, 04 (2006).
168. M. Jing, M. Ni, W. Song, J. Lu, Z. Gao, L. Lai, W. N. Mei, D. Yu, H. Ye, and L. Wang, *J. Phys. Chem. B* 110, 18332 (2006).
169. J. Li and A. J. Freeman, *Phys. Rev. B* 74, 075333 (2006).
170. Z. Y. Li and D. S. Kosov, *J. Phys. Cond. Matter* 18, 1347 (2006).
171. M. Nolan, S. O'Callaghan, G. Fagas, J. C. Greer, and T. Frauenheim, *Nano Lett.* 7, 34 (2007).
172. A. N. Kholod, V. L. Shaposhnikov, N. Sobolev, V. E. Borisenko, F. A. D'Avitaya, and S. Ossicini, *Phys. Rev. B* 78, 035317 (2004).
173. T. M. Schmidt, R. H. Miwa, P. Venezuela, and A. Fazzio, *Phys. Rev. B* 72, 193404 (2005).
174. T. Akiyama, K. Nakamura, and T. Ito, *Phys. Rev. B* 73, 235308 (2006).
175. S. P. Beckman, J. Han, and J. R. Chelikowsky, *Phys. Rev. B* 74, 165314 (2006).
176. J. Li and L.-W. Wang, *Phys. Rev. B* 72, 125325 (2005).
177. H. J. Xiang, J. Yang, J. G. Hou, and Q. Zhu, *Appl. Phys. Lett.* 89, 223111 (2006).
178. D. Karanth and H. Fu, *Phys. Rev. B* 74, 155312 (2006).
179. G. Shen, Y. Bando, C. Tang, and D. Golberg, *J. Phys. Chem. B* 110, 7199 (2006).
180. X. Chen, A. Nazzal, D. Goorskey, M. Xiao, Z. A. Peng, and X. Peng, *Phys. Rev. B* 64, 245304 (2001).
181. Y. Zhang, L.-W. Wang, and A. Mascarenhas, *Nano Lett.* 7, 1264 (2007).

182. R. T. Senger, S. Tongay, E. Durgun, and S. Ciraci, *Phys. Rev. B* 72, 075419 (2005).
183. L.-W. Wang, *Phys. Rev. Lett.* 88, 256402 (2002).
184. L.-W. Wang and J. B. Li, *Phys. Rev. B* 69, 153302 (2004).
185. X. Y. Huang, E. Lindgren, and J. R. Chelikowsky, *Phys. Rev. B* 71, 165328 (2005).
186. Y. Zhang (unpublished). We have found that by changing the bond lengths between the pseudo-H atoms and the host atoms, the surface levels could be tuned from below to above the band edge, and thus affect the band gap differently.
187. L.-W. Wang and A. Zunger, *J. Phys. Chem.* 98, 2158 (1994).
188. K. B. Wong, M. Jaros, and J. P. Hagon, *Phys. Rev. B* 35, 2463 (1987).
189. J. A. Brum, G. Bastard, L. L. Chang, and L. Esaki, *Superlattices Microstruct.* 3, 47 (1987).
190. D. S. Citrin and Y. Chang, *Phys. Rev. B* 40, 5507 (1989).
191. P. C. Sercel and K. J. Vahala, *Appl. Phys. Lett.* 57, 545 (1990).
192. P. C. Sercel and K. J. Vahala, *Phys. Rev. B* 44, 5681 (1991).
193. M. Tadić and Z. Ikonić, *Phys. Rev. B* 50, 7680 (1994).
194. S.-H. Park, D. Ahn, and Y.-T. Lee, *J. Appl. Phys.* 96, 2055 (2004).
195. K. Chang and J. B. Xia, *Phys. Rev. B* 58, 2031 (1998).
196. H. Sun, *Phys. Rev. B* 58, 15381 (1998).
197. Z.-Y. Deng, X. Chen, T. Ohji, and T. Kobayashi, *Phys. Rev. B* 61, 15905 (2000).
198. M. Tsetseri and G. P. Triberis, *Superlattices and Microstruct.* 32, 79 (2002).
199. D. M. Gvozdić and A. Schlachetzki, *J. Appl. Phys.* 92, 2023 (2002).
200. A. Siarkos and E. Runge, *Phys. Rev. B* 61, 16854 (2000).
201. Y. Zhang, *Phys. Rev. B* 49, 14352 (1994).
202. Z. Chen, Q. Gao, M. Ruan, and J. Shi, *Appl. Phys. Lett.* 87, 93113 (2005).
203. L. E. Brus, *J. Chem. Phys.* 80, 4403 (1984).
204. Y. M. Niquet, C. Delerue, G. Allan, and M. Lannoo, *Phys. Rev. B* 62, 5109 (2000).
205. A. B. Filonov, G. V. Petrov, V. A. Novikov, and V. E. Borisenko, *Appl. Phys. Lett.* 67, 1090 (1995).
206. B. X. Li, P. L. Cao, R. Q. Zhang, and S. T. Lee, *Phys. Rev. B* 65, 125305 (2002).
207. X. Zhao, C. M. Wei, L. Yang, and M. Y. Chou, *Phys. Rev. Lett.* 94, 219702 (2005).
208. F. Bruneval, S. Botti, and L. Reining, *Phys. Rev. Lett.* 94, 219701 (2005).
209. Y. F. Zhao and B. I. Yakobson, *Phys. Rev. Lett.* 91, 035501 (2003).
210. B. Marsen and K. Sattler, *Phys. Rev. B* 60, 11593 (1999).
211. R. Rurali and N. Lorente, *Phys. Rev. B* 72, 026805 (2005).
212. M. Bruno, M. Palummo, A. Marini, R. D. Sole, V. Olevano, A. N. Kholod, and S. Ossicini, *Phys. Rev. B* 72, 153310 (2005).
213. Y. Zhang, G. M. Dalpian, B. Fluegel, S.-H. Wei, A. Mascarenhas, X.-Y. Huang, J. Li, and L.-W. Wang, *Phys. Rev. Lett.* 96, 026405 (2006).
214. M. Zhao, Y. Xia, X. Liu, Z. Tan, B. Huang, C. Song, and L. Mei, *J. Phys. Chem. B* 110, 8764 (2006).
215. L. C. Lew Yan Voon, G. Galeriu, B. Lassen, M. Willatzen, and R. Melnik (unpublished).
216. A. H. Chin, T. S. Ahn, H. Li, S. Vaddiraju, C. J. Bardeen, C.-Z. Ning, and M. K. Sunkara, *Nano Lett.* 7, 626 (2007).
217. L. C. Lew Yan Voon and M. Willatzen, *J. Appl. Phys.* 93, 9997 (2003).
218. R. Melnik, M. Willatzen, L. C. Lew Yan Voon, and C. Galeriu, *Proc. ICCSA Montreal*, edited by C. T. V. Kumar, M. Gavrilova, and P. L'Ecuyer, ICCSS, Springer (2003), Vol. II, pp. 755–763.
219. M. P. Persson and H. Q. Xu, *Phys. Rev. B* 73, 035328 (2006).
220. J. Kim, L.-W. Wang, and A. Zunger, *Phys. Rev. B* 56, R15 541 (1997).
221. R. N. Musin and X.-Q. Wang, *Phys. Rev. B* 71, 155318 (2005).
222. R. N. Musin and X.-Q. Wang, *Phys. Rev. B* 74, 165308 (2006).
223. J. Hu, L.-W. Wang, L.-S. Li, W. Yang, and A. P. Alivisatos, *J. Phys. Chem. B* 106, 2447 (2002).
224. D. Katz, T. Wizansky, O. Millo, E. Rothenberg, T. Mokari, and U. Banin, *Phys. Rev. Lett.* 89, 086801 (2002).
225. D. Steiner, D. Katz, O. Millo, A. Aharoni, S. Kan, T. Mokari, and U. Banin, *Nano Lett.* 4, 1073 (2004).
226. X.-Z. Li and J.-B. Xia, *Phys. Rev. B* 66, 115316 (2002).
227. J. Li and L.-W. Wang, *Nano Lett.* 4, 29 (2004).
228. I. Vurgaftman, J. Hinckley, and J. Singh, *IEEE J. Quant. Elect.* 30, 75 (1994).
229. H. E. Ruda and A. Shik, *Phys. Rev. B* 72, 115308 (2005).
230. Y. Zhang, B. Fluegel, S. P. Ahrenkiel, D. J. Friedman, J. Geisz, J. M. Olson, and A. Mascarenhas, *Mat. Res. Soc. Symp. Proc.* 583, 255 (2000).
231. X.-Y. Wang, J.-Y. Zhang, A. Nazzal, M. Darragh, and M. Xiao, *Appl. Phys. Lett.* 81, 4829 (2002).
232. A. Shabaev and A. L. Efros, *Nano Lett.* 4, 1821 (2004).

Received: 14 June 2007. Accepted: 19 July 2007.